Photon time-of-flight and continuous-wave near-infrared-spectroscopy of human skeletal muscle tissue; a comparative study

Master's Thesis

By

Alfi Shaharin

Faculty of Engineering, LTH

Lund University, Sweden

ABSTRACT

The focus of this thesis is to perform a comparative study between two noninvasive optical techniques: Photon Time-of-flight Spectroscopy (pTOFS) and a Continuous-wave NIRS system for measuring muscle tissue oxygen saturation. INVOS 5100C (Manufactured in 2011, Serial Number 11-10269, Produced by Somanetics Troy, MI 48084 USA) is such a CW-NIRS system that provides tissue oxygenation using continuous wave Near Infrared Spectroscopy technique and widely used in the hospitals. Wide bandwidth time-of-flight spectrometer (pTOFS) based on photon time-of-flight spectroscopy is a fast and non-invasive instrument developed in the Group of Biophotonics, Lund University. This unique system is capable to deliver continues absorption/scattering spectra of turbid samples in a singularly broad wavelength range from 600nm up to 1400nm. It enables analysis of chemical composition and structural properties of turbid material like biological tissue, pharmaceutical tablets, food and agricultural products. The main idea of this technique is to send a very short pulse (ps regime) of light through the turbid sample and observe the temporal broadening of the injected short pulse. The broadening of the pulse then can be analyzed and the optical properties of the sample can be revealed. Thus it is possible to extract the optical properties of muscle tissue by implementing the same method. In the same way pTOFS was applied on human skeletal muscle tissue and a campaign was arranged for this after a written informed permission from the 21 healthy adult volunteer participants (8 women and 13 men).This campaign was approved by the Regional Human Ethics Committee at Lund University, Sweden. In the measurement the participant's right arm was extended with the palm facing upwards and the pTOFS sensor along with two CW-NIRS sensors were attached to it. The two wavelengths used in both the sensors were 730 nm and 810 nm. A blood pressure cuff was attached to the upper side of the arm to observe provocations such as immediate venous and arterial occlusion or progressive venous through arterial occlusion. From the CW-NIRS system tissue oxygenation based on both absorption and scattering effect were continuously obtained. While pTOFS provided the time of flight signals and evaluating these signals the optical properties i.e. the absorption coefficient and the scattering coefficient were estimated. Then by doing simple calculation using only the absorption coefficient it was possible to estimate the oxygen saturation. The oxygen saturation values for resting position obtained from CW-NIRS were in the range from 70-90%. From pTOFS it were in the range from 55- 60%, which is in the line with what is expected for normal physiology of muscle tissue [32][33]. By doing statistical analysis, StO_2 values during different provocations are compared with respect to their prior resting position. In both the techniques physiological changes with respects to StO_2 were observed. In clinical aspects monitoring of oxygen saturation in muscle tissues is very important. In critical conditions like brain injury and/or heart/kidney failure the muscle tissue saturation gets low as blood flow is increased towards the more important organs(like heart, brain and kidneys) from the less important organs like skeletal tissue etc. This functions as an indicator for the critical conditions. Hence proper steps can be taken to treat this type of clinical declining at an early stage. The unique ability of pTOFS to separate the absorption effect from the scattering effect gives more consistent StO_2 values. Despite this unique feature pTOFS instrumentation requires more research to be used for clinical measurement.

POPULAR SCIENCE

Optical spectroscopy is of great importance to determine the physical and chemical properties of a sample. When light of different colors (wavelengths) interacts with a material only certain colors are absorbed .That's why we see different colors of objects e.g. an apple looks red as it absorbs all other lights than red .This is the basic principle of absorption spectroscopy. The absorption of different color (wavelengths) by a material is related to the atomic and molecular structure of that material. Thus using the absorption spectroscopy it is possible to determine the chemical composition of a material. Absorption spectroscopy is convenient to use in the medium where light can travel in a rectilinear way e.g. in clear liquids, gas medium etc. However for the optical spectroscopy of highly scattering (turbid) materials like biological tissues, pharmaceutical tablets, milk, snow etc. it requires some additional consideration and complex methods of analysis. The amount of light that can be detected after passing through such a sample depends on both the scattering and the absorption properties of that material. Scattering occurs when photon changes its route after reflecting from the particles inside the medium. The Biophotonics group of Atomic Physics Division at Lund University is developing such a spectroscopic tool that can do optical spectroscopy of turbid materials and it is called Photon Time-of-Flight Spectrometer (pTOFS).The basic mechanism of the pTOFS technique is to observe the broadening of a very short laser pulse in time scale after passing through a turbid medium .Then this broadened pulse can be analyzed with proper mathematical model to extract the scattering and absorption properties of that medium. Each of these properties then can be used to obtain useful information of the medium.

The main focus of my thesis is to perform a comparative study between two optical spectroscopic techniques: Photon Time-of-flight Spectroscopy (pTOFS) and a Continuous-Wave Near Infrared Spectroscopy (CW-NIRS) system for measuring muscle tissue oxygen saturation (StO_2) in human. StO_2 is defined by the amount of oxygen bound to hemoglobin in the blood, expressed as a percentage of the maximal binding capacity. INVOS 5100C is a widely used CW-NIRS system which provides tissue oxygen saturation using continuous-wave Near-Infrared-Spectroscopy. The basic working principle of CW-NIRS is based on the absorption spectroscopy that doesn't count for the effect of scattering. Unlike CW-NIRS, pTOFS provides more relevant values of oxygen saturation as it is capable to separate the absorption properties from the scattering properties. These absorption properties are used to calculate the amount of oxygenated and deoxygenated hemoglobin in the blood as they absorb light of different wavelengths (colors).Then finally these amounts are the key data to calculate oxygen saturation.

Low tissue oxygenation values are directly related to many critical conditions like brain injury and/or heart/kidney failure. So, continuous monitoring of StO_2 works as an early indicator and helps the physician to take lifesaving steps in these conditions. In this regard pTOFS can be applied more reliably than CW-NIRS as it has the unique capability to use only the absorption effect. But unlike the CW-NIRS system, pTOFS instrumentation still needs further development to apply it in clinical measurement.

ABBREVIATIONS

VIS	Visible
NIR	Near infrared
pTOFS	Photon Time of Flight Spectroscopy
CW-NIRS	Continuous Wave Near Infrared Spectroscopy
DA	Diffusion Approximation
DE	Diffusion Equation
IRF	Instrumental Response function
APD	Avalanche Photo Diode

Contents

Chapter 1

INTRODUCTION

The spectroscopy of turbid (highly scattering) materials like tissue in NIR regions is very important in the field of bio-photonics, and biomedical applications. The motivation of this thesis is to perform a comparative study between the two noninvasive optical techniques: Photon Time-of-flight spectrometer (pTOFS) developed in the Group of Biophotonics, Lund University, and a Continuous Wave near Infrared Spectroscopy system for measuring Muscle tissue saturation. Reliable monitoring of oxygenation in muscle tissues can detect poor tissue oxygenation clinically. Muscle tissue saturation gets low for critically ill patients as blood flow is increased towards more important organs like heart, brain and kidneys. This can be an indicator for brain injury and/or heart/kidney failure. Hence proper steps can be taken to treat this type of clinical declining at an early stage. Hemoglobin in body tissue transports oxygen from lungs to the cells of the body and the oxygenation of the tissue is found by dividing the oxygenated hemoglobin by total amount of hemoglobin. So,

$$\text{Tissue Saturation, } StO_2 = \frac{[HbO2]}{[Hb]+[HbO2]} * 100\%$$

Continuous wave NIRS system is a standard technique widely used in the hospitals for measuring muscle tissue saturation and key method of this system is conventional absorption technique with continuous light source. INVOS 5100C is such a system. The fundamental form of NIRS is that it applies the Beer-Lambert Law of light attenuation in tissue to calculate the concentration of absorbing chromophores, generally de-oxygenated and oxygenated hemoglobin. Two wavelengths are used to determine the concentration change of these two chromophores [23]. However, this spectroscopic technique has limitations in measuring turbid materials where optical path length is unknown due to multiple scattering events. Wide bandwidth Photon Time-of-Flight Spectroscopy (pTOFS) is such an approach which enables the determination of the optical properties i.e. scattering and absorption separately. Unlike conventional spectroscopy pTOFS requires sensitive instrumentation for photon detection and proper physical model for propagation of photon into the medium for extracting correct optical properties .Thus pTOFS considers the unknown path length distribution and the geometrically determined losses of light due to scattering [4]. That's why justifying the implementation of Photon Time-of-Flight Spectroscopy (pTOFS) for measuring muscle tissue saturation is a very new and important approach. Photon time-of-flight spectroscopy can also be used for characterization of highly scattering materials such as biological tissue, pharmaceutical samples, food and agricultural products and so on.

To perform the study the instrumental setup of photon time-of-flight spectroscopy (pTOFS) system was optimized. The main idea of using the pTOFS technique is to send a very short pulse (ps regime) of light through the turbid sample and observe the temporal broadening of the

injected short pulse. Values on tissue oxygenation were continuously obtained from the CW-NIRS and from the pTOFS the time-of-flight signals were obtained. The pTOFS was optimized in such a way that it has the same source-detector arrangement as INVOS5100C system. The optical properties i.e. the absorption coefficient and the scattering coefficient were estimated by evaluating the pTOFS signals and doing simple calculation using the absorption coefficient the oxygen saturation was estimated. The oxygen saturation values in resting position obtained from CW-NIRS were in the range from 70-90%. The oxygen saturation values obtained from pTOFS were in the range of 55- 60%, which agrees more with the normal physiology of muscle tissue [32][33]. Statistical analyses are done to show how different provocations change the StO_2 values with respect to its prior resting position.

Chapter 2

BASIC PHYSICS OF LIGHT MATTER INTERACTION

Any media that consists of particles which absorbs or scatters light can be termed as turbid media. When light travels through these media some of it will be reflected from the surface while the rest will be either absorbed or scattered.

2.1 Scattering: Biological origins

Scattering can be of two types: Elastic-no change in photon energy e.g. Rayleigh scattering and Mie scattering and Inelastic scattering. Inelastic scattering phenomena such as Raman and Brillouin scattering involve energy exchange between the photon and the molecule [2]. Chemical composition as well as the molecular structure of the biological tissue can be revealed by Raman scattering. On the other hand elastic scattering can reveal the size distribution of the scatterers. As the inelastic scattering process is much weaker than elastic scattering, processes such as Raman and Billirouin scattering can be ignored in this context [1]. Elastic scattering in turbid material originates from the non-uniformities in refractive index. If in a scattering medium the scatterers are distributed randomly in space, multiple scattering events takes place. When the scatterers are distributed in such a way that the distance between different particles is much greater than both the particle size and the incident wavelength then single scattering theory applies to the scattering event.

2.1.1 Scattering by a single Scatterer:

When a plane wave is incident on a scattering particle it creates a new field being distorted by the scatterer. The resulting field is a sum of the incoming field and the scattered field [4]. The scattered field may be characterized by a single parameter called the differential cross section $\partial\sigma_s$. The angular distribution of the power of the scattered field i.e. the Poynting vector of the far field scattered field is described by this parameter.

Scattering cross section σ_s can be yield by integrating the differential cross section over all solid angles

$$\sigma_s = \int_{4\pi} \partial\sigma_s \, d\omega' \tag{2.1}$$

Suppose a medium have many scatterers with number density ρ_s , the scattering coefficient i.e. the total cross sectional area for scattering per unit volume can be interpreted as

$$\mu_s = \sigma_s \rho_s \tag{2.2}$$

The scattering coefficient illustrates the probability of the interaction that takes place with the scatterers per unit length. When a plane wave is propagating in a specific direction in a scattering medium and travelled an infinitesimal length Δx the intensity lost can be interpreted as

$$dI = -\mu_s \Delta x \, I \tag{2.3}$$

The amount of scattering in a medium or in a biological structure is described by the scattering coefficient μ_s and this amount is strongly related to the optical wavelengths. If the particle size of the interacting medium or the biological structure matches with the optical wavelength then the medium or the structure functions as a very highly scattering medium.

2.1.2 Multiple scattering:

Multiple scattering can be explained by the figure below:

a)

b)

c)

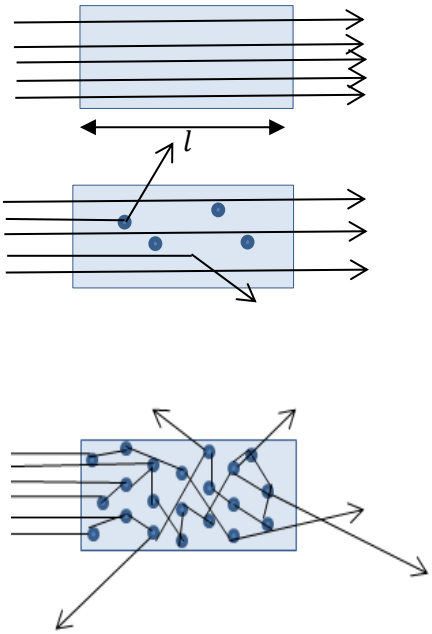

Figure 2.1: Light propagation in different samples [4]

In Figure 2.1 a) There is no scatterer, light passes through, in b) the sample is a dilute suspension of the scatters , rays are scattered only once, this is the single scatterer regime in c) rays are scattered multiple times, this is multiple scatterer regime where only scattered rays are transmitted [4]. There a lot of everyday objects that has properties like c). Like cloud, milk,

snow, white paint, pharmaceutical tablets and so on owe their white appearance to multiple scattering.

The scattering coefficient can be defined considering multiple scattering as follows:

$$l = \frac{1}{\mu_s} \tag{2.4}$$

The mean free path may be interpreted by considering the scattered propagating as a wave outwards from the scattered and a direction $\hat{\boldsymbol{s}}$. The mean free path is the average distance the scattered field propagates in that direction before it encounters a new scatterer. If the mean free path is much longer than the wavelength of light, the scattered wave is approximately equivalent to a plane wave when it encounters the next scatterer.

For high scattering material, like tissue, it is required to define scattering by reduced scattering coefficient μ_s' = (1-g)μ_s , where, g is the anisotropy coefficient and used to describe the angular distribution of the light scattering. The scattering and absorption properties are strongly wavelength dependent and the stronger the absorption, the smaller the penetration depth of that particular wavelength.

2.3 Absorption:

Absorption happens when the energy of a photon is matched with the energy gap between the initial and final states. Absorption in tissue originates from different kinds of molecules and biomolecules. The ultraviolet region is strongly absorbed by most of the materials, so the optical penetration is much shorter in this region which makes it less interesting in turbid material spectroscopy. Detailed discussion on absorption in tissue and on the optical window where the penetration depth is much higher for biological tissue is discussed in Chapter 5.

The absorption coefficient μ_a is the probability that a photon is absorbed in a medium per unit path length. Light attenuates when it propagates in an absorbing-only medium according to the following equation

$$\frac{dI}{I} = -\mu_a dx \tag{2.5}$$

Where, I = injected light intensity

And, x is the distance the light travels along the propagation direction. The absorbed energy is considered to be lost.

2.4 Photon Time of Flight Spectroscopy:

Many turbid medium like biological tissues are highly affected by scattering when light of specific wavelengths propagate through them and the optical path of the photons become unknown. Using absorption spectroscopy, absorption measurement of such materials is rigorously affected

by the scattering and it is not possible to decouple absorption and scattering properties. One of the possible ways to distinguish between absorption and scattering in measurement is to make photon-time-of-flight spectroscopy (pTOFS). In this technique, the detected signal is evaluated not only considering the absorption, but also considering the unknown path length distribution and the geometrically determined losses of light due to scattering .The main idea of this technique is to observe the broadening of the injected short laser pulse passing through the medium. A very short laser pulse (in picoseconds regime) is injected into the medium and collected at some distance from the injection point (Figure 2.2).

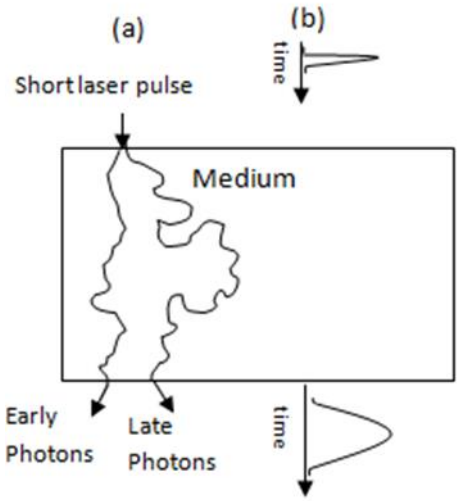

Figure 2.2 : (a) Random photon propagation, transmitted photons can be classified as early or late according to their time of flight through the medium.(b) A short pulse gets temporally broadened during passing through a scattering medium.

It is observed that when light is allowed to propagate through such a scattering material, different photons arrive at the detector travelling different distances with different time of-flights (TOF). So, the resulted pulse becomes broadened. The higher is the scattering in the medium the wider is the broadening of the pulse.

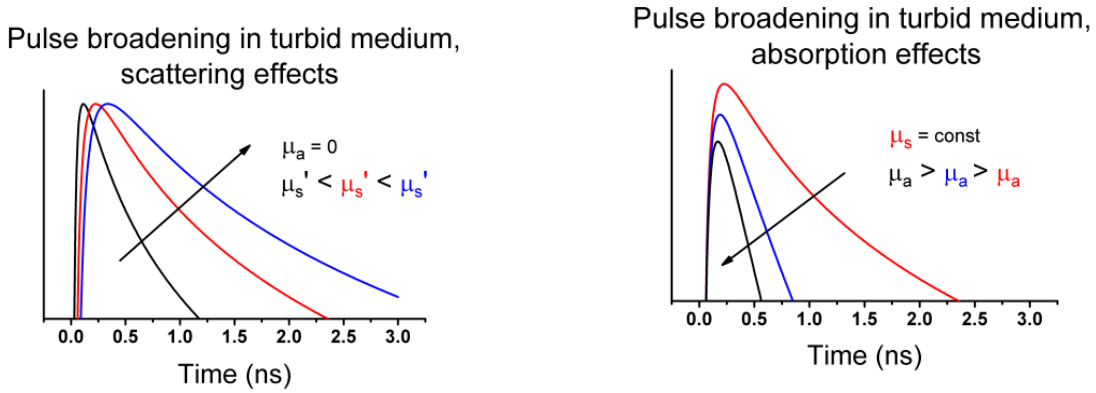

Figure2.3: Pulse broadening in the turbid medium [16]

The pulse gets narrower when the medium is absorptive as well. As, the late photons travelling have higher probability to be absorbed in the medium.

Chapter 3

Theory of Photon Migration and Radiative Transport Theory

The microscopic Maxwell equations can easily describe the fundamental behavior of electromagnetic fields. However, in turbid materials such as biological tissue the transport of light on a macroscopic scale can be impossible to describe by Maxwell equations. When light enters into such highly diffusive medium, the optical path of the photons becomes unknown due to the multiple scattering events. Radiative transfer theory (RTT) effectively models this multiple scattering. RTT is based on the arguments of energy conservation.

3.1 Radiative Transfer Equation :

The Radiative transfer equations (RTE) can be formulated by using macroscopic optical properties i.e. the scattering coefficient $\boldsymbol{\mu_s}$ **, the absorption coefficient** $\boldsymbol{\mu_a}$ and the scattering phase function $p(\hat{\mathbf{s}}', \hat{\mathbf{s}})$. RTE is also referred to as the Boltzmann transport equation.

The RTE express the balance of energy inside a volume element of the scattering medium. The RTE can be obtained by considering the total space and time variation of the specific intensity along a direction $\hat{\mathbf{s}}$ in an elementary volume and making this equal to the variation of specific intensity due to scattering and absorption inside the medium [19]. The final equation for the time dependent case is:

$$\frac{1}{v}\frac{\partial}{\delta t} I(\boldsymbol{r}, t, \hat{\mathbf{s}}') + \hat{\mathbf{s}}' \nabla I(\boldsymbol{r}, t, \hat{\mathbf{s}}) = -\mu_t I(\boldsymbol{r}, t, \hat{\mathbf{s}}) + \frac{\mu_t}{4\pi}\int_{4\pi} p(\hat{\mathbf{s}}', \hat{\mathbf{s}}') I(\boldsymbol{r}, t, \hat{\mathbf{s}}') d\omega' + \varepsilon(\boldsymbol{r}, t, \hat{\mathbf{s}}) \qquad (3.1)$$

Where,

$I(\boldsymbol{r}, t, \hat{\mathbf{s}}')$ = The specific intensity or energy, moving in the direction $\hat{\mathbf{s}}$, per unit of solid angle, per unit of time, and per unit of area normal to the $\hat{\mathbf{s}}$ direction [19].

$v =$ The speed of light inside the diffusing medium,

$\mu_t = \mu_s + \mu_a$ = The loss of radiance out of each infinitesimal volume element defined by the scattering coefficient μ_s and the absorption coefficients μ_a respectively.

$\varepsilon(\boldsymbol{r}, t, \hat{\mathbf{s}})$ = The source term and

$p(\hat{\mathbf{s}}', \hat{\mathbf{s}}) =$ The scattering function that defines the probability for a photon scattered in the direction $\hat{\mathbf{s}}$, to be scattered into direction $\hat{\mathbf{s}}'$.

3.2 Solving the Radiative Transport Equation (RTE) with Diffusion approximation:

The **RTE** is solved with numerical methods or analytical approximations. The diffusion approximation (DA) can be used to simplify the RTE for some sample geometries such as infinite medium, semi-infinite medium and slab medium. In this modeling only elastic scattering is considered such that the scattering event changes the direction of the photon but does not change its frequency. The absorbed energy is completely lost. Under certain conditions RTE reduces to a simple diffusion equation.

To obtain the diffusion equation (DE) in order to build the DA model, source is considered as isotopic that emits a pulse of unit energy, $Q(r,t) = \frac{1}{4\pi} * \delta(r - r')\delta(t)$. The following assumptions are also considered:

1. In DA it is assumed that the specific intensity encounters many particles inside the medium and is scattered almost uniformly in all directions i.e. it is assumed to be almost isotropic. However for the propagation of power the angular dependence is not constant, so the diffuse flux vector $F_d(\boldsymbol{r}, t)$ is nonzero. In other words the diffuse intensity is slightly more in the direction of the net flux flow than in the backward direction. Mathematically the specific intensity is approximated with the first two terms of a Taylor's expansion in terms of the power of $\hat{\boldsymbol{s}}_{\boldsymbol{forward}}.\hat{\boldsymbol{s}}$ [17].

$$I(\boldsymbol{r}, t, \hat{\mathbf{s}}) = U_d(\boldsymbol{r}, t) + \frac{3}{4\pi} F_d(\boldsymbol{r}, t).\hat{\mathbf{s}}' \tag{3.2}$$

Where,

$U_d(\boldsymbol{r}, t) = \frac{1}{4\pi}\int_{4\pi} I(\boldsymbol{r}, t, \hat{\mathbf{s}}) d\omega$ is the average diffuse intensity and

$F_d(\boldsymbol{r}, t) = \int_{4\pi} I(\boldsymbol{r}, t, \hat{\mathbf{s}}).\hat{\boldsymbol{s}} d\omega$ is the diffuse flux vector.

This assumption is also called as P1 approximation.

2. The phase function $p(\hat{\mathbf{s}}', \hat{\mathbf{s}})$ is assumed to depend only on the scalar product $\hat{\mathbf{s}}.\hat{\mathbf{s}}'$.

3. The time variation of the diffuse flux vector over a length of $\mathbf{1}/\boldsymbol{\mu_s}'$ is assumed to be negligible with respect to the vector itself.

These simplifying assumptions and the integration the RTE multiplied by $\hat{\boldsymbol{s}}$ over all solid angles leads to the Fick's law.

$$F_d(\boldsymbol{r}, t) = -4\pi D \Delta U_d(\boldsymbol{r}, t) \tag{3.3}$$

By applying the Fick's law we get the diffusion equation for a homogeneous non-linear medium as,

$$\left(\frac{1}{v}\frac{\partial}{\delta t} - D\nabla^2\right) U_d(\boldsymbol{r}, t) = Q(\boldsymbol{r}, t) \tag{3.4}$$

The validity of the photon diffusion model (equation (3.1)) depends on the validity of the first approximation which describes that the radiance to be nearly isotropic. This isotropy is achieved when scattering coefficient $\mu_s \gg$ the absorption coefficients μ_a .

Now, the different solutions of this equation which are obtained including absorption effect for an infinite medium, a semi-infinite medium with different boundary conditions will be discussed only for the time resolved system.

3.3 Boundary Conditions:

When a light source irradiates a small spot i.e. a narrow collimated pulsed light beam is normally incident (along z axis) on the surface of a semi-infinite medium or slab medium from the outside , it is reasonable to model such a source as an isotropic source at a depth z_o (Figure 3.1), typically, $z_o = 1/\mu'_s$ [3]. It is assumed that all incident photons are initially scattered at this depth below the surface. For a diffusing medium bounded by a surface, the exact boundary condition or the zero boundary condition can be considered when there is no mismatch between the refractive index of the diffusing medium and that of the surrounding medium and in this case, at the surface there should be no diffuse light entering the medium. In short the average diffuse intensity (fluence rate) is equal to zero at the physical boundary [19]. This condition is no longer valid when a refractive index mismatch occurs. The refractive index mismatch is considered in extrapolated boundary condition. In this boundary condition the average diffuse intensity (fluence rate) is not zero at the physical boundary of the medium rather there is a zero-crossing point for the fluence rate at a distance, z_e, outside (i.e., on the air side) of the medium.

$$z_e = 2AD \tag{3.4}$$

Where, the coefficient *A* is given by

$$A = \frac{1 + 3\int_0^{\pi/2} R(\theta_i) cos^2(\theta_i) \sin(\theta_i)\, d\theta_i}{1 - 2\int_0^{\pi/2} R(\theta_i) \cos(\theta_i) \sin(\theta_i)\, d\theta_i} \tag{3.5}$$

θ_i = the angle of incidence of the radiation and

$R(\theta_i)$ = the Fresnel reflection coefficient for un-polarized light.

3.3.1 Infinite-Medium:

Considering a short isotropic pulse $Q(r,t) = \frac{1}{4\pi} * \delta(r - r')\delta(t)$ the resulting average diffuse intensity for the simplest case where no boundaries need to be taken into account i.e. for infinite medium geometry is

$$U_d(\boldsymbol{r},t) = \frac{v\exp(-\frac{|r-r'|^2}{4Dvt})}{4\pi(4\pi Dvt)^{3/2}} \quad (3.6)$$

Where, $D = \frac{1}{3\mu_s(1-g)} = \frac{1}{3\mu_s'}$, is the diffusion coefficient.

By taking account of Beer-Lambertian attenuation feature i.e. by multiplying $\exp(-\mu_a vt)$ the equation gets the form as below:

$$U_d(\boldsymbol{r},t) = \frac{v\exp\left(-\frac{|r-r'|^2}{4Dvt} - \mu_a vt\right)}{4\pi(4\pi Dvt)^{3/2}} \quad (3.7)$$

It is clear from the above equation that It should be noted that the time resolved system can be used to measure both absorption and scattering without the need for absolute measurements.

3.3.2 Semi-infinite Medium:

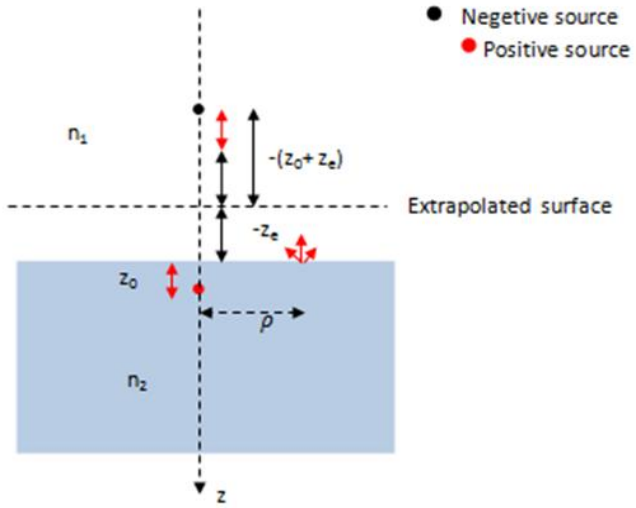

Figure 3.1: Semi-infinite homogeneous medium for diffused reflectance [16]

For semi-infinite medium the time resolved diffused reflectance

$$R(\rho,t) = \frac{\exp\left(\mu_a vt - \frac{\rho^2}{4Dvt}\right)}{2(4\pi Dv)^{3/2}t^{5/2}} \times \left[z_0 \exp\left(-\frac{{z_0}^2}{4Dvt}\right) + (z_0 + 2z_e)\exp\left(-\frac{(z_0+2z_e)^2}{4Dvt}\right)\right] \quad (3.8)$$

Where, μ_a = absorption coefficient of the diffused medium

$v = \frac{c}{n_2} =$ velocity of light in the defused medium

$D = \frac{1}{3\mu_s'}$ is the diffusion coefficient.

$t =$ time

$\rho =$ distance of collection fiber from the z axis

3.4 Modeling by Monte Carlo Simulation:

Unfortunately, several turbid mediums exhibit optical properties in the range where the use of the diffusion approximation may not be implemented. For example the human prostate which exhibits that the reduced scattering coefficient is much lower than the absorption coefficient. Again, when the fiber separation is small then the analytical photon diffusion is not applicable. In such conditions for the data evaluation, an advanced data fitting algorithm based on Monte Carlo (MC) simulations is used. Applying the MC method to the radiation transport equation is about tracing particles from the source to the turbid medium. Then inside the medium the particles are absorbed and scattered until they exit the region of interest. If this method is applied repeatedly for a large numbers of particles, the traces for these particles may be used to estimate how the entire population behaves in the medium. Thus for a large number of photon packages, it is possible to obtain statistics for the absorption and scattering [20].

3.5 Data Evaluation and Fitting of Experimental Data with Theoretical Model:

In Photon Time of Flight spectroscopy, the signal is evaluated analyzing the temporal broadening of the pulse using above mentioned theories and boundary conditions. In this technique, temporal response of pTOFS curve is acquired first and then the optical properties corresponding to that curve are sought in an iterative way. Consequently, a set of parameters (i.e. $p(\hat{\mathbf{s}}', \hat{\mathbf{s}}), \mu_s \; and \; \mu_a$) is very essential for a specific medium geometry with particular refractive index mismatch between this medium and its surrounding. Here, at first a theoretical model pulse is convolved with the Instrumental Response Function (IRF) (Figure 3.2) and this convolved pulse is tried to fit with experimentally acquired broadened pulse by iteration process. IRF is achieved by sending the short laser pulse through the system without any sample in such a way that the perturbation caused by the sample remains the same. In other words IRF accounts the temporal broadening of the system which can be caused by the optical components and instruments like fibers, detectors etc.

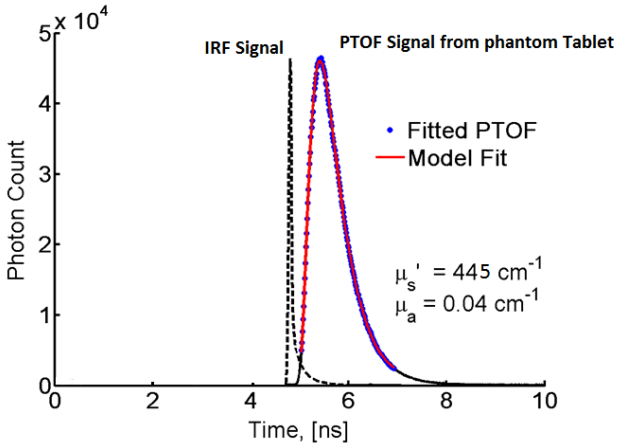

Figure 3.2: Time reference and IRF [16]

A very common and popular method for iterative minimization of the sum of squares is the Marquardt-Levenberg method [20]. The method turns to achieve the minimization of the function

$$\tilde{\chi}^2(\mu_a, \mu_s') = \sum_{i=1}^{N} \left(\frac{y_i - y(\mu_a, \mu_s', t_i)}{\sigma_i}\right)^2 \quad 3.9$$

Where,

$y_i = experimental\ data$

$t_i = corresponding\ time$

$\sigma_i = wieghts\ of\ the\ data\ points$

$y(\mu_a, \mu_s', t_i) = model\ prediction$

The model prediction is the convolution of the theoretical impulse response and the IRF. However, when diffusion model breaks down (e.g. in the case where absorption is comparable to scattering or fiber distance is very small), White Monty Carlo is used for modeling. The basis of this fitting procedure is to find the optimal choice of μ_a for each value in a set of trial values of μ_s' [21]. The search can be done with a finite resolution of $\Delta\mu_s'$. For each μ'_s value, the optimal values of μ_a and a free scalar parameter, k are determined using Marquardt-Levenberg minimization of the error norm:

$$\tilde{\chi}^2 = min_{k,\mu_a}\{\chi^2(k, \mu_a, \mu_s')\ \} \quad (3.10)$$

Chapter 4

Photon Time-of-flight Spectroscopy: Instrumental setup

4.1 Introduction:

The Photon Time of Flight Spectrometer (pTOFS) consists of the following units:

1. Super Continuum Fiber Laser Source
2. Acousto Optic Tunable Filter
3. Optical Fibers
4. Detectors
5. Time-correlated Single Photon Counting Electronics(TCSPC)

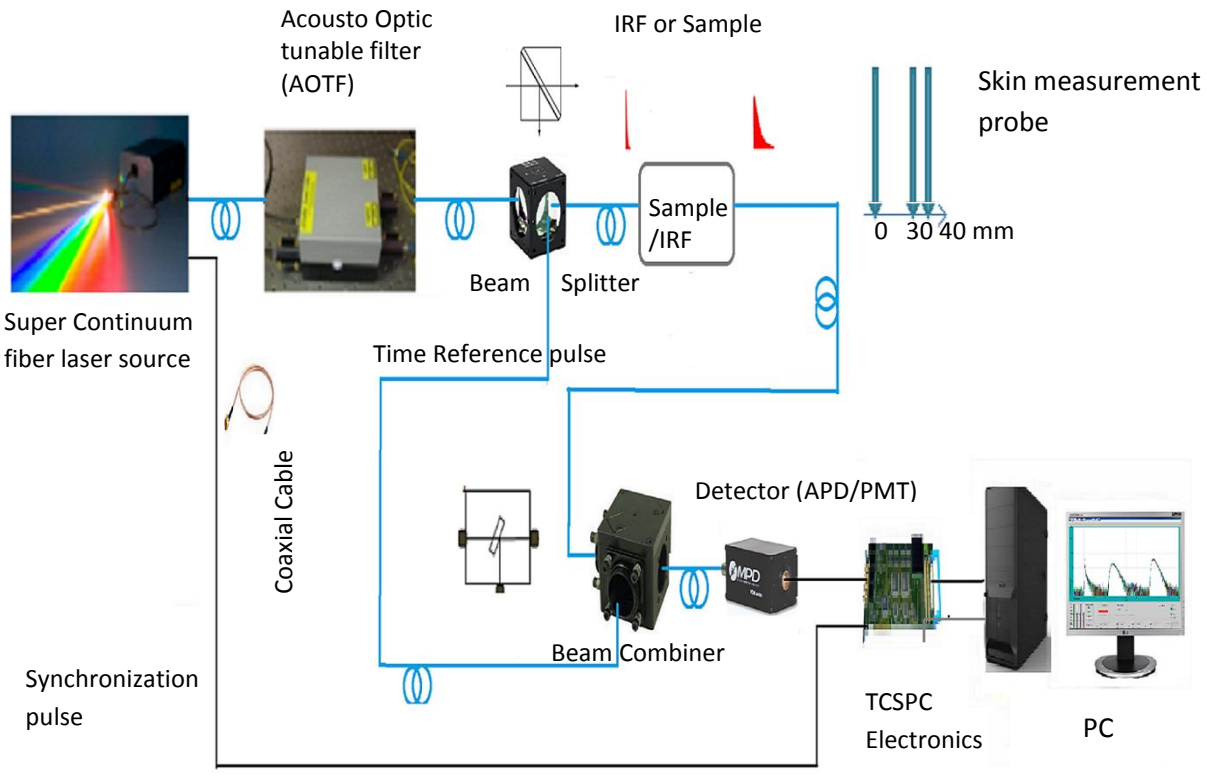

Figure 4.1: Photon time of flight spectrometer set up (detailed)

4.2.1 Super Continuum Fiber Laser Source :

Photon Time-of-Flight Spectrometer gives absorption and scattering spectra of turbid samples in a singularly broad wavelength range from 600 nm up to 1400 nm. Super continuum fiber laser

source provides light pulse with a wide spectral bandwidth ranging from 500 to 1850 nm with repetition rate of 80 MHz. The maximum optical power > 3mW/nm (spectral density). The ytterbium (Yb) doped fiber laser generates pulses of 6.0 ps (oscillator pulse width) .The source consists of a high power laser diode pumping device. With higher amplification rates both the optical output power and the spectral bandwidth are increased. A broad spectrum is then generated in a supercontinuum generator which is consists of a non-linear photonic crystal fiber (PCF). This is a special type of optical fiber with a built-in microstructure of arrays of holes arranged in a periodic manner. The air holes change the fiber's waveguide properties are changed by the air holes as the refractive index changes with the propagation of light [10]. The broadening of the spectra is a non-linear process; the spectra will first be extended to longer wavelengths, i.e. greater than 1064 nm which in turn will generate the shorter ones, below 1064 nm [11].

4.2.2 Acousto Optic Tunable Filter:

The wide bandwidth white light from the super continuum source is transmitted through a GRIN fiber to Acousto-Optical Tunable Filter. It is used to transmit light pulse of narrow band at particular wavelength. The basic principle of working is that the refractive index of a birefringent crystal changes when it is exposed to an acoustic wave [12]. According to Bragg condition:

$$\sin\theta = \frac{\lambda}{2\Lambda}$$

$\theta = angle\ of\ the\ incoming\ light$

$\lambda = wavelength\ of\ the\ light$

$\Lambda = acoustic\ wavelength$

When both the angle θ and the acoustic wavelength Λ are known, reflection of the incident light of particular wavelength will only occur in the medium as all the other optical wavelengths will be refracted in other directions and eventually will disappear. This wavelength selection property is used to filter desired wavelength. The refractive index of the crystal is varied by using a piezoelectric transducer. The light with the selected wavelength is collected by a fiber placed in a pinhole. By choosing different vibration frequency of the piezoelectric transducer by an AOTF-driver (controlled through a computer), the acoustic wavelength is changed. From 650nm to 1100nm the AOTF sends pulses with bandwidth 3-6nm and with bandwidth 6-12nm in the range of 1100nm to 1850nm [13].

4.2.3 Optical Fibers:

When light comes into an ordinary optical fiber with different angles, it travel with different speeds and the detected signal will be temporally broadened. In pTOFS setup this broadening can be much larger than the signals detected. Thus the accuracy would decrease completely. To avoid this, graded index fibers of 400 µm core diameter (cladding diameter- 600 µm) are used instead [16] . The numerical aperture of the fiber is 0.27 and the active area diameter of the

single-photon avalanche photo – detector (SPAD) is matched with that of the fiber. In these fibers the refractive index has a parabolic profile i.e. the core refractive index decreases with increasing radial distance from the fiber axis. So, light travels in slower velocity at the center and gradually increases the velocity with radial distance. Thus the temporal broadening can be very efficiently avoided by using this type of fibers.

4.2.4 Detectors :

From Figure 4.1 Photon time of flight spectrometer set up, it is observed that after proper selection of the wavelength, the source light from AOTF is divided into two pulses with the help of a beam splitter. One of them is timing reference pulse(with attenuated optical power) which directly goes to the beam combiner and the other pulse i.e. the pTOFS signal pulse goes through the sample or IRF and then to the combiner. After combining in the Beam Combiner these pulses are sent to the detector. Depending on the wavelength region selected by the AOTF driver through a computer two types of detectors are used. One of them can cover from 600nm to 1000nm while the other can detect light ranging from 1000 nm to 1400 nm. For 600 nm to 1000 nm region a Single – Photon avalanche photodiodes (SPAD) detector called PMD100ct from *MICRO Photon Devices* is used. Its photon detection efficiency is about 49% at 550nm which is obtained through the use of epitaxial silicon Single Photon Avalanche Diodes (SPAD) [14]. The active area diameter is 100µm the detection range is from 400nm to 1000nm.

For the NIR spectral range between 1000-1400 nm a Micro-Channel Plate Photo Multiplier Tube (MCP-PMT) with InP/InGaAsP photocathode (R3809U-68 from Hamamatsu Photonics) is used. Being extremely sensitive to room light MCP-PMT needs to be operated in a dark room. To reduce the thermal noise and to increase the sensitivity of the detector it requires cooling down to -80^{o}C. Then the output signal is amplified by HFAC-26, Becker & Hickl, amplifier, which also controls a shutter that protects the detector from overloading. The cooling system used is a R3809U-50/1406 from Research Inc. For cooling, liquid nitrogen is pumped from a Cryogenic storage dewar and this pumping is controlled by the temperature. The pumped liquid nitrogen is freed automatically at the point of required temperature and thus the temperature remains constant. An air tight lid (Aluminum ring) is prepared for the dewar to avoid any external pressure is required for pumping the nitrogen.

4.2.5 Time-correlated Single Photon Counting Technique:

Time-correlated single photon counting (TCSPC) is an exceptionally sensitive technique for recording low-level light signals with picosecond resolution and extremely high precision based on the detection of individual photons, the measurement of the detection times, and the reconstruction of the waveform from the individual time measurements [15]. TCSPC makes use of the fact that for low-level, high-repetition rate signals the light intensity is usually low enough that the probability to detect more than one photon in one signal period is negligible.

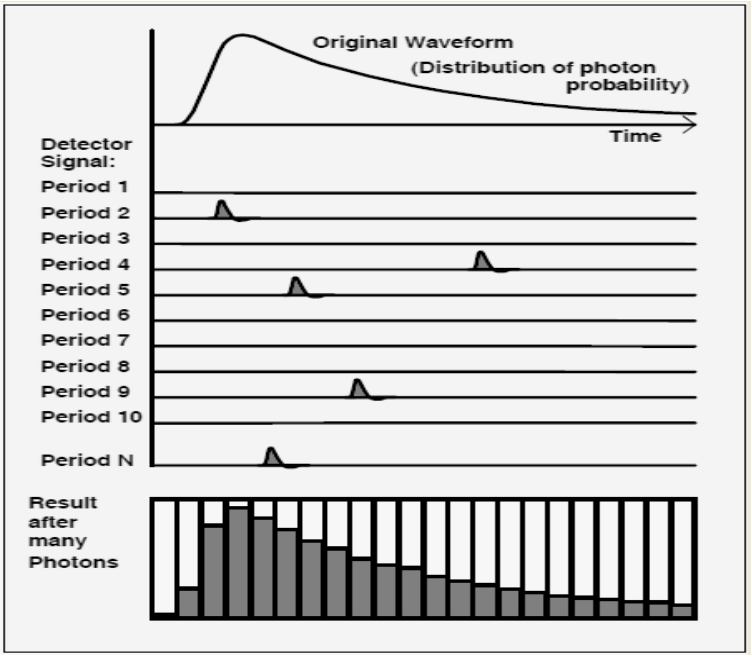

Figure 4.2 Basic Principle of Time correlated single photon counting [15]

Basic Principle:

When a photon is detected, the arrival time of the corresponding detector pulse in the signal period is measured. The events are collected in a memory by adding a '1' in a memory location with an address proportional to the detection time. After many signal periods a large number of photons have been detected, and the distribution of the photons over the time in the signal period builds up distribution of the photon probability.

In our setup as TCSPC electronics, SPC-130 module from "Becker & Hickl GmbH" is used. The module contains complete electronic systems such as the Constant Fraction Discriminators (CFDs), the Time-to-Amplitude Converter (TAC), a fast Analog-to-Digital Converter (ADC), the data processing logics, and the data memory which are integrated on the Board.

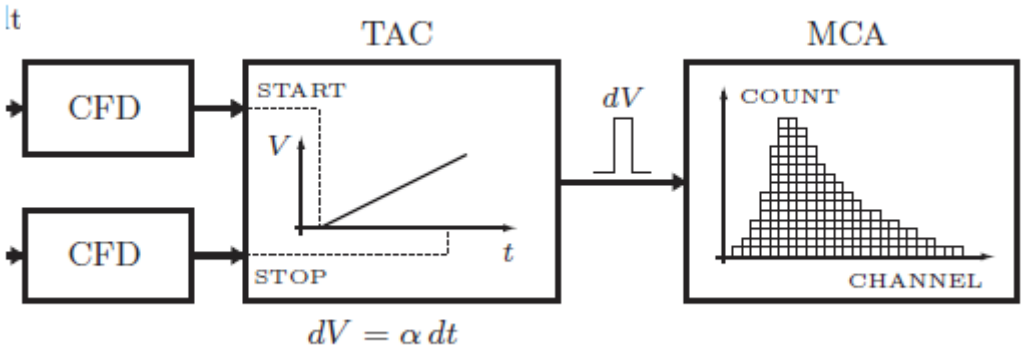

Figure 4.3: A schematic of a typical TCSPC setup [22].

When a photon reaches the detector a signal is sent to one of the constant *fraction discriminator* (CFD). A second CFD is also used to obtain a synchronization pulse from the light source. The CFD improves the timing of the system by compensating for fluctuations in the amplitude of the

signals and helps to reduce the noise in the measurement by excluding pulses with too high or low amplitude (noise from the detector and electronics). The ”normalized” pulse is then sent to the TAC and triggers the converter and starts an internal clock in the TAC. The TAC clock is started when a single photon is detected and stopped with the next synchronization pulse from the light source reaches. The time interval between these two pulses is converted into an electrical pulse that has amplitude which is directly proportional to the time delay. Conventional TACs use a switched current source for charging a capacitor. The start pulse switches the current on while the stop pulse switches it off. The voltage (proportional to time difference) of the electrical pulse is then sent to multichannel analyzer. After several repetitions of the same event a statistical histogram is created which represent a photon time-of-flight distribution (Figure 4.3). That means the no. of photons is distributed at different time channels where each photon detected from a particular sample pulse.

So, instead of acquiring the overall photon distribution, the TCSPC technique generates a histogram describing the distribution of the earliest photon. When the light intensities are higher, the optical signal must be attenuated before it reaches the detector [16]. Which means in practice it is only a small fraction of the injection pulses that produce a detection event. Using high repetition-rate pulsed lasers will allow fast generation of proper histogram [17].

4.3 Timing reference pulse and IRF Measurement:

Precise timing calibration is very important in time of flight spectroscopy [18]. The temporal drifts, introduced by the source (mainly responsible), detector and the finite resolution of the TCSPC detection, results error in measurement and leads to poor precision in optical properties. This problem can be resolved by implementing double path optical scheme in the setup to measuring the fraction of direct laser pulse simultaneously with the IRF and the pTOFS signal [16]. This fraction of direct laser pulse is called timing reference pulse.

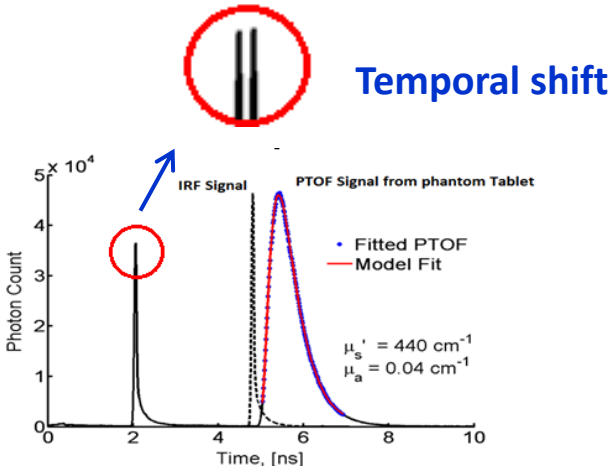

Figure 4.4: Temporal Shift in timing reference pulse

The timing reference pulses for pTOFS signal and IRF pulse must have exactly the same shape and ideally their peaks should come exactly at the same point if there is no jitter in system. So, the difference between their peak positions must reflect the temporal shift in measurement. By

adding or subtracting this temporal shifting value, one can get the correct position of the IRF and pTOFS signal and measure correct absorption (μ_a) and scattering coefficients (μ_s').

Chapter 5

Optimizing the Instrumental Setup for Muscle Tissue Saturation in Humans

5.1 Introduction:

Biological tissue contains a large number of different chromophores such as hemoglobin, lipids, water, and melanin and so on. These behave differently in different spectral range. Like in the visible and ultraviolet range they can behave as very highly scattering and absorbing molecules. To avoid high absorption and to have a maximum penetration depth in the order of milli- to centimeters an optical window in the near infrared range exists. This tissue optical window is primarily limited by absorption of different tissue chromophores such as hemoglobin at shorter wavelengths ($\lambda < 600\ nm$) and water for longer wavelengths ($\lambda > 1000\ nm$).

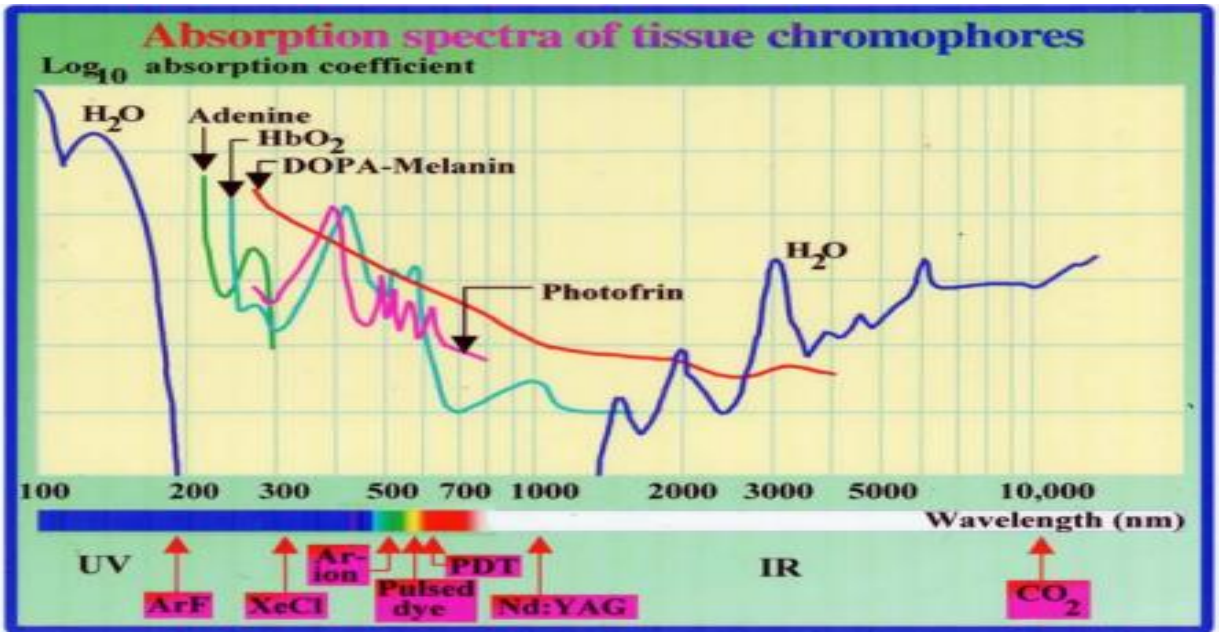

Figure 5.1: The absorption spectra and the tissue optical window [24]

5.2 Near-Infrared spectroscopy (NIRS): A non-invasive optical technique to monitor the physiology of muscle tissue

For imaging and distinguishing the physiological properties of tissues, extensive research had been done so far to develop noninvasive optical techniques. Diffuse optical Near Infrared Spectroscopy is such a non-invasive optical technique that provides the opportunity to apply absorption spectroscopy to a highly scattering medium like human tissue. It uses the light in the

near infrared spectrum (700-1000 nm) where it's propagation in tissue is dominated by scattering. It merges experimental measurement and model-based data analysis to measure the absorption and scattering properties of cm-thick tissues and then can lead to the prediction and monitor of subject's response to different therapies. New detection technologies and smart algorithms using multispectral imaging techniques are getting more interesting in this field of diagnostics.

This is an effective technique for studying biochemical state of tissue. Information about the changes in tissue saturation as a result of increase in blood flow due to exercise (active hyperemia) or due to stress (reactive hyperemia) can be analyzed by this technique [5].

Hemoglobin, a chromophore that has wavelength dependent absorption of photons is of vital importance as it is the carrier of oxygen from the lungs to the cells of the body. When the hemoglobin molecule is bound to oxygen then it is called as oxy-hemoglobin or $Hb0_2$. If the hemoglobin molecule is bound to nothing then it is deoxy-hemoglobin or Hb. These two have different spectra. This property is the basis of the pulse oximeters. With the help of modified Beer-Lambert law the actual saturation in the microcirculation of the tissue can be approximated.

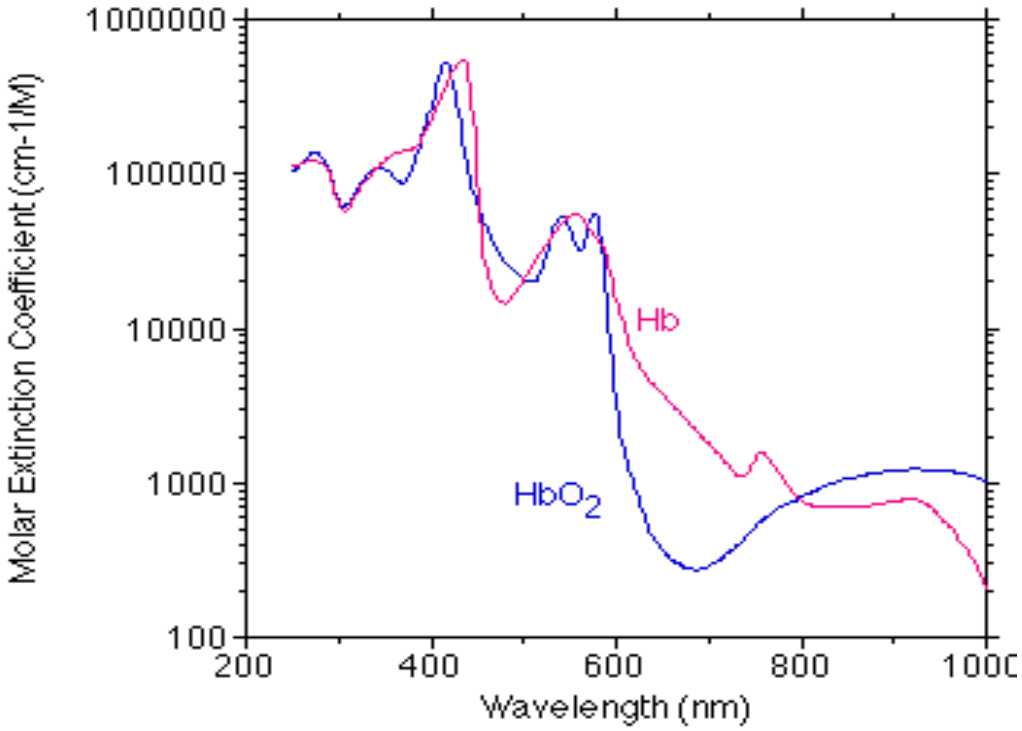

Figure5.2: Spectrum for Hb (deoxygenated hemoglobin) and HbO_2 (Oxygenated hemoglobin) [6]

NIRS is sensitive to the vessels with diameter of $< 100\ \mu m$ i.e. arterioles, capillaries and venules as light reaching vessels with a diameter of >100 μm is absorbed completely [7]. So, this technique mainly reflects capillary-venous oxygen saturation.

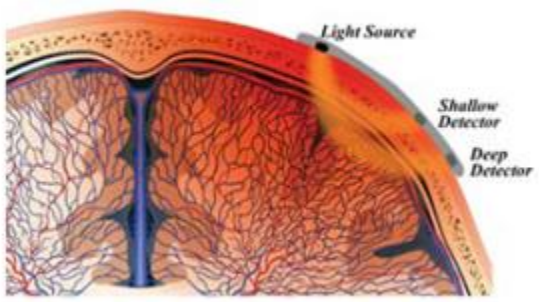

Figure 5.3: Detectors spacing and photon paths [25]

After the light penetrates into the skin it is absorbed by hemoglobin and some fraction of the photons can survive after several scattering events and thus can return to the skin. If photons at deeper location are to be probed detectors should be placed further away from injection point. Thus by measuring and analyzing the quantity of returning photons as a function of wavelength information regarding tissue oxygen saturation (StO_2), concentration of total, oxygenated and deoxygenated hemoglobin (Hb) can be found. The main loss mechanism of photons is absorption, and it is measured by the loss of the injected intensity after passing through the sample and following Beer-Lambert law of absorption.

According to Beer-Lambert law:

$$I(L) = I_o \exp(\mu_a L)$$

Where initial photon intensity of light before passing through the sample, L is path length, $I(L)$ is intensity of light after passing through the sample and μ_a is the absorption coefficient of the medium.

For non-scattering medium it is easy to calculate the path length. However, for scattering medium it is not feasible due to multiple scattering events. Applying conventional absorption spectroscopy in scattering medium, only extinction spectra can be obtained which is the interplay of absorption and scattering.

5.3 The comparative study of two non-invasive optical techniques: *Continuous wave Near Infrared Spectroscopy –INVOS 5100C* and *Photon Time –of-Flight Spectroscopy*

Materials, Subjects and Methods:

The study was carried out in the Division of Atomic Physics at the Faculty of Engineering (LTH), Lund University, Sweden. The campaign was started after the approval of the Regional Human Ethics Committee at Lund University, Sweden. A written informed permission was obtained from the 21 healthy adult volunteer participants (8 women and 13 men).The participants were selected anonymously after ensuring that they meet the inclusion criteria which was justified by doing usual clinical examination (e.g. listening to the heart, measuring arterial blood pressure) by

doctors and the participants' history regarding any cardiovascular problems, medical illness, medications and allergies were noted. Two doctors were always present during the whole period of study. The participants were not allowed to exercise heavily, drink coffee and /or alcohol or to use tobacco 24 hours before the measurement starts. The right forearm was used for the measurements as the subcutaneous fat tissue layer in this arm is relatively thin. The skinfold thickness of the proximal ventral right forearm was measured by a caliper and half of the value was used to estimate the thickness of the fat tissue covering the muscle. Participants were mixed in skin types and the individual type was evaluated by following a Fitzpatrick skin type chart [9]. This is the most commonly used scheme to classify a person's skin type by their response to sun exposure in terms of the degree of burning and tanning was developed by Thomas B. Fitzpatrick, MD, PhD.

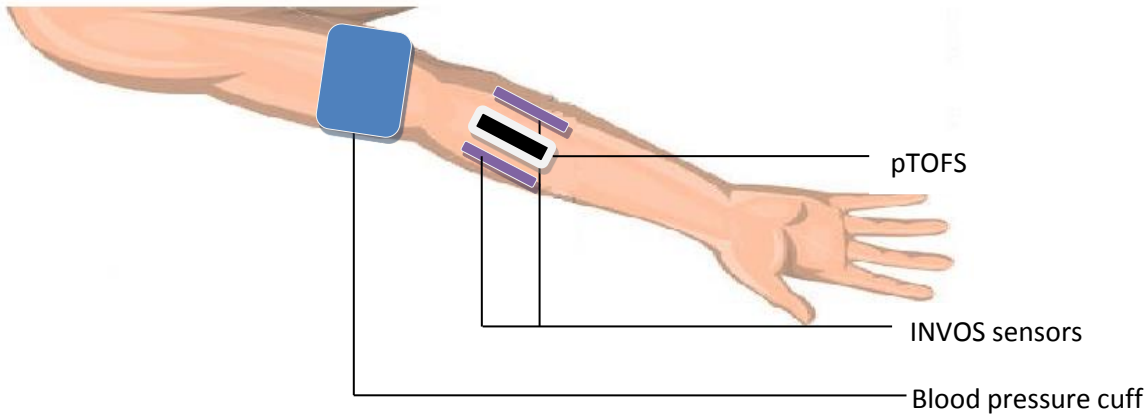

Figure 5.4 Schematic diagram of the setup

During the measurement each patient was resting on a bed with the head of the bed raised up to some extent. INVOS 5100C was always monitored at the other end of the bed. The right arm of the patient was extended on the bed while keeping the palm of the hand facing upwards [Figure 5.4]. Two self-adhesive sensors from the CW-NIRS (INVOS) were attached on the lower forearm of the hand (In anatomical terms of location the proximal ventral area of the right lower arm). The photon time-of-flight sensor was attached with surgical tapes between the two sensors. For monitoring of non-invasive arterial oxygen saturation (SpO2) a pulse oximeter probe was positioned on a fingertip (of the index finger) on the left hand. The pulse oximeter was also providing the pulse rate. A blood pressure cuff (Size 12x35) was fastened as shown in figure. Using the cuff, provocation such as immediate venous occlusion or progressive venous through arterial occlusion was done. While placing the sensors, large veins were avoided as the detected signal had low photon count (for photon time of flight spectroscopy) i.e. absorption was high in such regions. The depth of the tissue region from the source to the detector was the same in pTOFS as in the CW-NIRS system and it can be estimated that the depth is half of the distance between the source and detection probes [31], the effective sampling depth in this study was

between 15 and 20 mm. The preparation took about twenty minutes. The whole study took about 90 minutes.

INVOS 5100C

INVOS 5100C uses continuous wave Near Infrared Spectroscopy system to provide tissue oxygenation. Light in two different wavelengths (730 nm and 810 nm) is generated by INVOS sensor and pass through the scalp or bone tissue beneath the sensor. For each of these wavelengths the sensor has two detector spacing: a shallow (3 cm) and a deep (4 cm) [Figure 5.5] i.e. at each distance the detectors could detect the two wavelengths simultaneously.

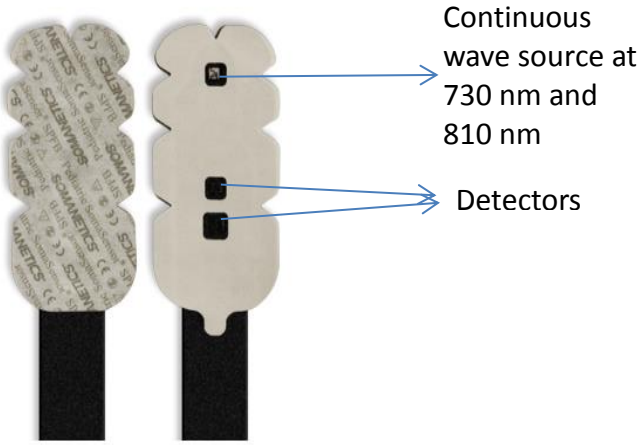

Figure 5.5: INVOS Sensors

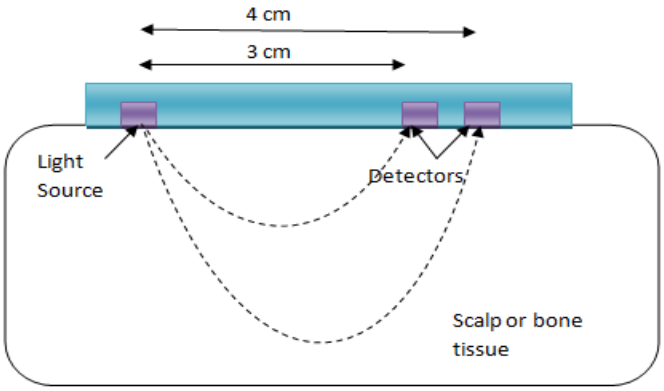

Figure 5.6: Tissue beneath INVOS sensor

Oxygen saturation for the specific deeper tissues beneath the source –detectors region is achieved by subtracting the signal (figure 5.6) of the shallow detector (3 cm) from that of the deeper detector (4 cm) [8].

Photon Time of Flight Spectroscopy

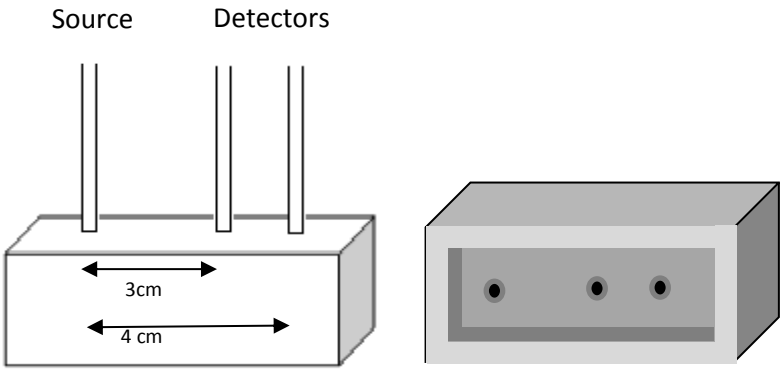

Figure 5.7 pTOFS Sensor

The setup for pTOFS was slightly changed from the basic setup (Figure 4.1, Chapter 4). As we have to detect signals at two different distances, one more beam combiner was introduced in the optical path to combine the signals from these distances. The remaining part was the same. For detecting the time reference and the pTOFS signals, the APD detector (detection range of wavelength is from 650nm to 1 microns) was used. The data from the detector was acquired by Time Correlated Single Photon Counting (TCSPC) electronics and sent to PC for analyzing the photon-time-of-flight distribution.

pTOFS sensor and the two sensors of CW-NIRS were positioned in such away such that the crosstalk between them was kept in a minimum level. By observing the detected time of flight signals it was easy to decide where to place the CW-NIRS sensors. The source in each CW-NIRS sensor increased the noise level in the detected signals if they were placed incorrectly. Values on tissue oxygenation were obtained from the CW-NIRS and from the pTOFS the time of flight signals at two different distances were obtained.

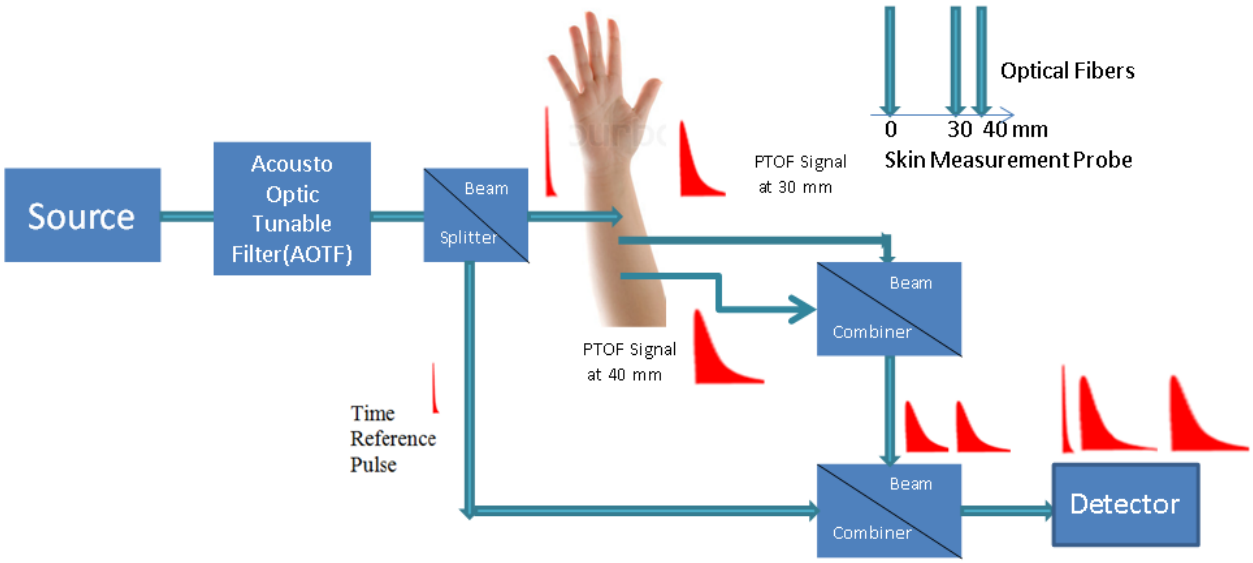

Figure 5.8: pTOFS setup for oxygen saturation measurement

Fiber distance:

It is important to calculate the pTOFS source and detection probe fibers distance so that different signals (e.g. time reference and pTOFS/IRF) appear at least with reasonable distance in time domain view of the TCSPC window.

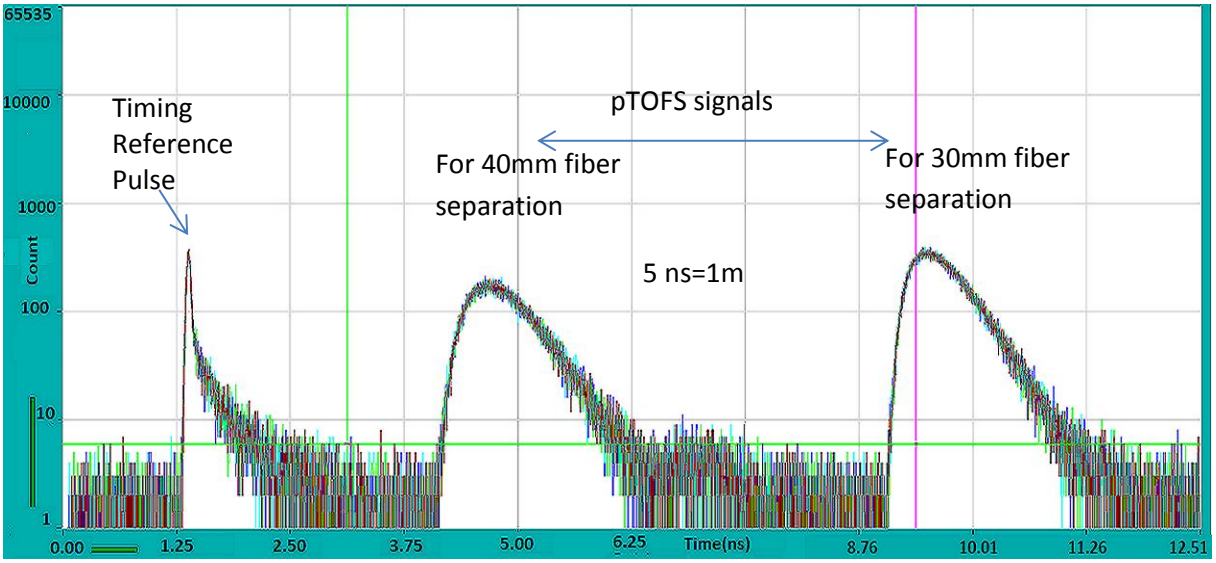

Figure 5.9: pTOFS signals and time reference pulse in the TCSPC window

As the source has a repetition rate of 80MHz our TCSPC window is limited to 12.5ns (1/80Mhz). The two pTOFS signals were fitted in such a way that they had approximately 5ns peak to peak distance from each other in the time domain. The idea behind selecting this distance is that each pTOFS signal should get enough space (in the time domain) to be broadened without overlapping. To make this difference between the signals the fibers were cut to have a difference in distance of approximately 1 m. On the other hand, as the temporal width of the timing reference pulse has no chance to be broadened, the peak to peak distance between the timing reference pulse and first pTOFS doesn't need to be large enough.

During designing different fiber length, the attenuation due to fiber was also considered. The longer the fiber distances, the higher the attenuation of signal output. Again, The pTOFS signal also becomes weak with the increased distance between the source and the detection fiber probes. That's why it was wise to use the shorter fiber at a distance of 40mm and the longer one at a distance of 30mm from the source fiber. For particular refractive index (n = 1.5) of the optical fiber, it was calculated that, 5 ns distance in time = 1 m distance in fiber length. So the fiber at 30mm is 1m longer than that at 40mm. The coaxial cable from the detector connected to the PC also contributes to shift in time and adding 1m of co-axial cable will give 4.94625 ns (calculated from TCSPC window) shift in time. So, the length of the coaxial cable was fixed first and then the fiber lengths were customized by calculating the approximate lengths to fit in the TCSPC window.

5.4 Physiological Situations:

The measurement was started as soon as the set up was ready. There were four different physiological situations in the whole study protocol. Directly before and after every physiological provocation baseline recordings were conducted (Figure 5.10, **C**). During baseline the patient was simply laid down without any provocations .The whole measurement procedure had five such baselines. It was very important to have baseline before and after every new study situation as it was possible to verify the physiological stability by returning to the StO_2 of baseline measured in real time with CW-NIRS. Each baseline was of ten minutes of duration. These ten minutes were maintained for both the system at the same time i.e. the stop and start time of these ten minutes were maintained in a similar way for both the techniques. This was a bit tricky to do. So one person was always with the continuous-wave system (INVOS) to maintain this. Using the pulse oximeter, continuous values on arterial saturation and pulse rate were obtained non-invasively. These values were registered once for every new study events. Four different physiological situations:

I) change in leg positioning,
II) immediate venous occlusion,
III) progressive venous through arterial occlusion , and
IV) Immediate arterial occlusion,

were studied using CW-NIRS and pTOFS .Throughout the study protocol, for the four different physiological situations with one of the situations having five different steps and for the five baseline measurements (in Figure 5.10 shown as **C**), in total thirteen different optical study events were recorded (Figure 5.10).

The different situations are discussed briefly below:

I. Change in leg positioning (Leg-lift): Following ten minutes of baseline measurement the volunteer resting in a horizontal position lifted his leg with the help of others. It lasted for ten minutes. It was important that the volunteer shouldn't put any effort to lift their legs as the goal was to observe the increased blood flow towards the heart during this time. The legs were lifted to a 60 degree angle and were hold by some lifted support. The legs were attached to the support using a plastic band to keep them in a resting position.

II. Immediate venous occlusion: Following ten minutes of baseline measurement just as above an immediate venous occlusion of 60 mmHg around the upper right arm was obtained using the blood pressure cuff. The duration of this occlusion was of ten minutes, and during these ten minutes StO_2 values from the CW-NIRS technology was obtained. From the pTOFS system Time-of-flight signals were obtained and saved for further simulation.

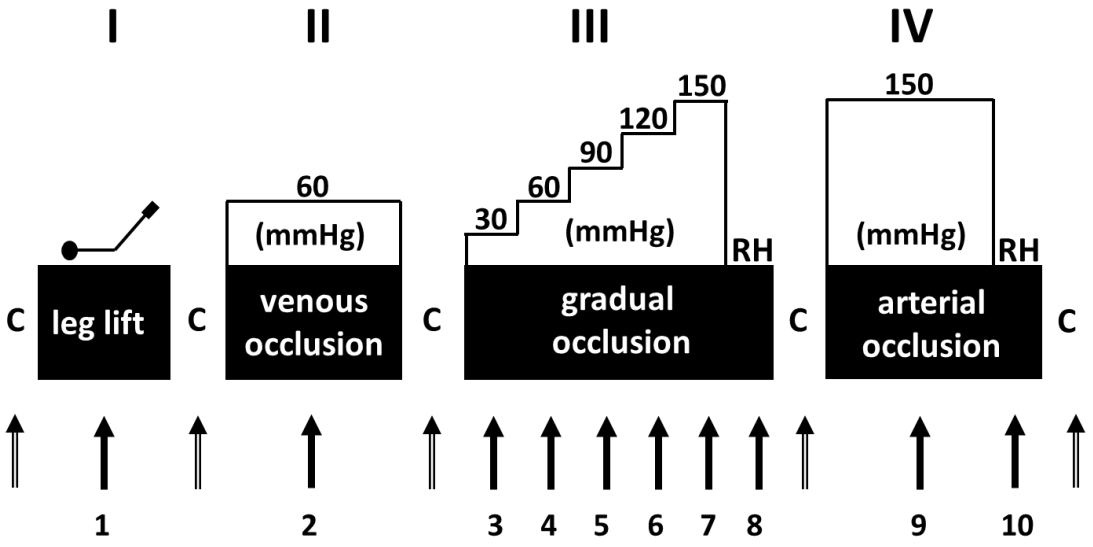

Figure 5.10 Different Physiological Situations [26]

III. Progressive venous through arterial occlusion : Following a ten minutes baseline just as above gradual venous through arterial occlusion was started from 30 mmHg and ended at 150 mmHg with the steps of 30 mmHg was obtained by gradually increasing the pressure using the above mentioned cuff. Each of these occlusions lasted for three minutes, so in total fifteen minutes of occlusion were done. The two optical study techniques were simultaneously providing corresponding optical output at

each level of measurements. Optical measurements were also recorded just after the cuff was released. In medical term it is called reactive hyperemia which means increase in blood flow after temporary interruption.

IV. Immediate arterial occlusion: Again following a ten minutes of baseline measurement an immediate arterial occlusion of 150 mmHg was conducted for five minutes and the optical data was recorded from the two different techniques. Then immediately after the release of the occlusion the effect (Reactive hyperemia) was recorded which lasted for couple of minutes and the measurement was continued for ten minutes to return the normal position.

Chapter 6

Data handling

6.1 Data handling in CW-NIRS (INVOS 5100C) system:

As discussed in Chapter 5 in section 5.3 the CW-NIRS sensor i.e. INVOS 5100C sensor has continuous-wave sources that can produce light of 730 nm and 810 nm wavelength at the same time. For both of these sources the sensor contains four detectors at two distances i.e. at 3 and 4 cm (See Figure 5.5). Eventually each sensor provides one set of data regardless of the data received at two distances in the sensor. In our experiment we used two sensors and got two sets of such data. The frequency at which the data points were updated automatically by the INVOS 5100C system was of 6 seconds. So, in ten minutes of measurement one can get around 100 data points. There was an exception to this situation when data points were taken at a frequency of 30 seconds. This was due to some software bug in the system and was not controllable. But it happened only in the case of two volunteers. Consequently StO_2 values obtained from these two volunteers were discarded for analysis.

6.2 Data handling in Photon Time of Flight Spectroscopy (pTOFS) system:

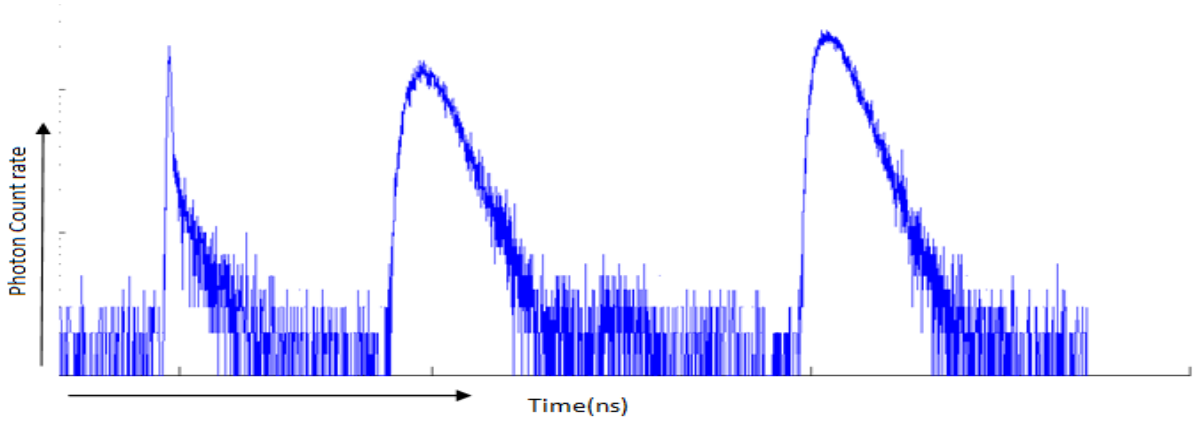

Figure 6.1: Photon time of flight output, the first signal from the left corresponds to the time reference pulse, the next two pulses are from the muscle tissue detected at 4 and 3 cm respectively

In case of Photon Time of Flight spectroscopy signals at two different distances were obtained (Figure 6.1). As the signals were obtained by changing the wavelengths manually the data processing time was different for pTOFS compared to CW-NIRS system. It took about 30 seconds to obtain a full set of data i.e. signals for two wavelengths at two distances were saved within 30 seconds of time. So, in ten minutes it was possible to get 16 data points for each wavelength. During the measurement, different photon count rate of pTOFS signal was found for different

patient at different physiological situations. That's why IRFs' were measured corresponding to those count rates before starting the measurement (It could also be possible to take IRF immediately after the measurement). It is very important to measure the pTOFS and IRF at the same photon count rate regime so that detector behaves similarly for both signals. The optical properties i.e. the absorption coefficient μ_a and the scattering coefficient μ_s' were estimated by implementing the evaluation algorithm based on diffusion approximation. As the tissue was surrounded by air the refractive index mismatch is needed to be considered, and this was done by implementing the extrapolated boundary condition. The refractive index of the tissue was assumed as 1.4 and the medium was considered as semi-infinite.

6.2.1 Photon count rate and thickness of subcutaneous fat layer: Discarding some measurements

It was quite obvious that the low photon count rate was obtained while taking the arterial occlusion (Cuff pressure of 150 mmHg). This was due to increased amount of trapped blood in the measurement area under the blood pressure cuff. As 150 mmHg was quite high pressure (blood pressure range for a healthy person is 120/80) there were less amount of new blood from the heart and as a result the volume of blood was almost unchanged as the cuff worked as a closed valve. On the other hand, the person having thicker layer of subcutaneous fat provide higher photon count rate due to higher scattering property of fat. Reasonably, count rate for measuring pTOFS signal were different for different physiological situations. For the few first studies, the photon count rates for the pTOFS and IRF signals were not properly maintained and it provided erroneous results for pTOFS data evaluation. Consequently, from the whole study of twenty one healthy volunteers seventeen were taken. One of the measurements was also discarded due to human errors while measuring the provocations.

6.2.2 Calculating Tissue Saturation (StO_2) from pTOFS

By doing simple calculation using molar extinction coefficient [6] of HbO_2 and Hb and the absorption coefficient μ_a for the wavelengths (730 nm and 810 nm), [HbO_2] and [Hb] is obtained. Where, [HbO2] and [Hb] refer to molar concentration of oxygenated hemoglobin and de-oxygenated hemoglobin respectively.

Absorption coefficient = molar concentration *molar extinction coefficient Or,

$$\begin{bmatrix}\mu_a(\lambda_1)\\ \mu_a(\lambda_2)\end{bmatrix}=\begin{bmatrix}C_{Ox}\\ C_{deOx}\end{bmatrix}*\begin{bmatrix}\varepsilon_{Ox}(\lambda_1) & \varepsilon_{deOx}(\lambda_1)\\ \varepsilon_{Ox}(\lambda_2) & \varepsilon_{deOx}(\lambda_2)\end{bmatrix}$$

Where, $C_{Ox} =$ [HbO_2], C_{deOx} = [Hb], $\varepsilon_{Ox}(\lambda_1)$ =Molar extinction coefficient of HbO_2 at λ_1, $\varepsilon_{deOx}(\lambda_2)$ =Molar extinction coefficient of Hb at λ_2

These molar concentration values are then used to calculate tissue saturation. As, tissue saturation is defined as,

$$StO_2 = \frac{[HbO2]}{[Hb]+[HbO2]} * 100\%$$

Chapter 7

Results and discussions

7.1 CW-NIRS (INVOS 5100C) output: Tissue Saturation(StO_2)

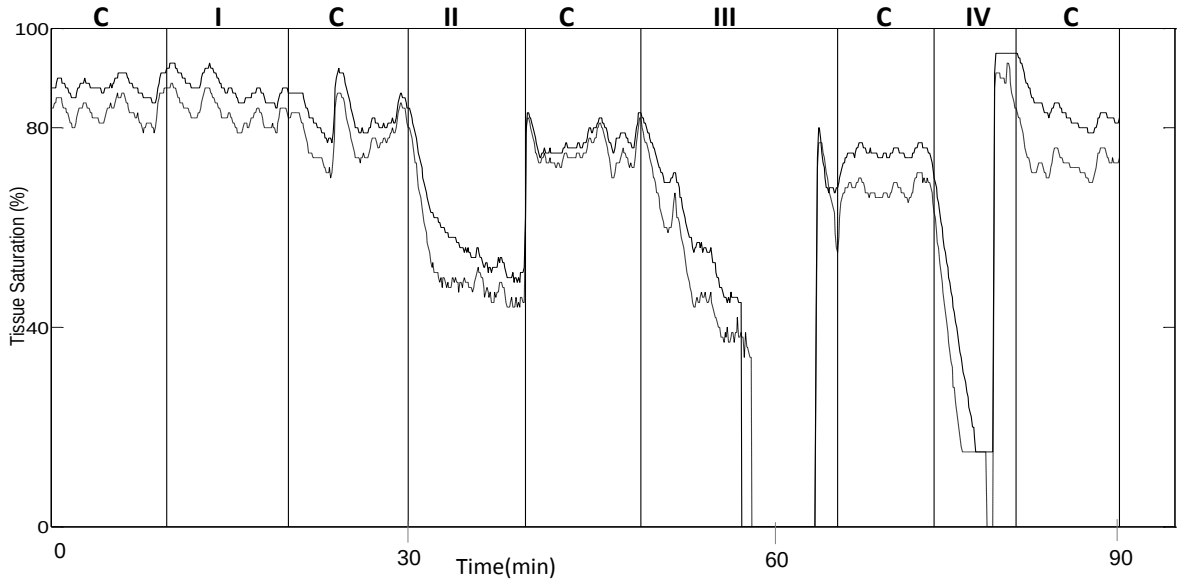

Figure 7.1 CW-NIRS (INVOS 5100C) Tissue Saturation output for one volunteer for different physiological situations (**I to IV**) with corresponding baseline (**C**) before each situations

Figure 7.1 shows the tissue saturation output from the CW-NIRS system used in the experiment for one participant. The two curves were obtained continuously from the two sensors used in the participant's right arm along with the pTOFS sensor (See Figure 5.4). As discussed in the previous chapter there are four different physiological situations (See in Figure 7.1 from **I to IV**)

I. change in leg positioning (Leg lift)
II. immediate venous occlusion(Cuff 60 mm Hg)
III. progressive venous through arterial occlusion(Gradual occlusion) , and
IV. Immediate arterial occlusion (Cuff 150 mm Hg).

Before each situations a ten minutes baseline (Shown in Figure 7.1 as **C**) was conducted. It is noticeable from the figure that at the last stage of Gradual Occlusion (**III**) the CW-NIRS output was zero. It means INVOS 5100C cannot measure extremely low oxygen saturation (below 15 %).

7.2 Photon time of flight Spectroscopy (pTOFS) outputs :

Absorption and Reduced Scattering Coefficient

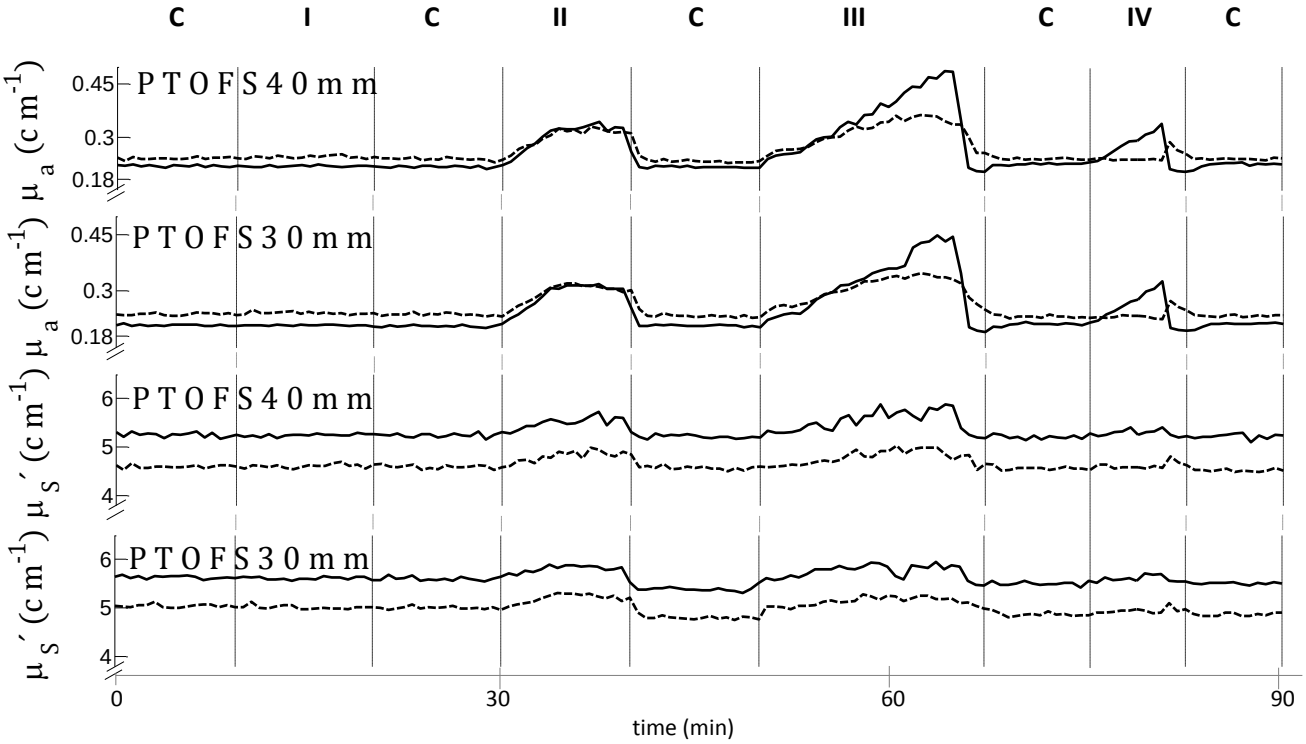

Figure 7.2 : Absorption coefficient (μ_a) and reduced scattering coefficient (μ_s') for different physiological situations (**I to IV**) with corresponding baseline (C) before each situations at two distances (30 and 40 mm) for 730nm (solid lines) and 810 nm (dashed lines) for one volunteer using pTOFS[26]

From Figure 7.2 the absorption coefficient is higher in **II** i.e. in the immediate venous occlusion of Cuff 60 mm Hg for both the wavelengths. The explanation can be discussed from the molar extinction coefficient values [6]. Molar extinction coefficient is a measure how strongly a substance absorbs light at a particular wavelength. The molar extinction coefficient is higher for Hb at 730 nm than for HbO_2. Again, at 810nm it is slightly higher for HbO_2 than for Hb. Absorption coefficient goes high when the total concentration of hemoglobin is higher [2] and at cuff pressure of 60mmHg the venous blood (but not arterial)is almost occluded [27] thus the total concentration increases.

In the case of **III** i.e. at progressive venous through arterial occlusion (Gradual occlusion) the inflation was started from 30 mmHg and with a step of 30 it was inflated till 150 mmHg. Figure 7.2 shows that in **III** the absorption coefficient at 810nm was almost unchanged from 90 mmHg to 150 mmHg and for 730nm it is increasing in a gradual manner. The effects can be explained in the way that just after 60mmHg the cuff starts to occlude the oxygenated arterial blood and at 150mmHg the forearm is totally cut off from new oxygenated blood (HbO_2). From 90 mmHg till 150mmHg the amount of HbO_2 didn't increase. Now, as absorption is higher for HbO_2 at 810nm, the 810nm curve was almost smooth during this inflation range. Also at this range the trapped

volume of blood contains more Hb than HbO_2 as O_2 has dissociated from HbO_2 and diffused away and consumed by the body cells. This explains the fact that the absorption coefficient at 730nm goes gradually higher as absorption is higher for Hb at 730nm. The physiological situation at **IV** where 150mmHg of pressure was applied immediately can be explained in the same way.

The scattering coefficient didn't change significantly for the different types of occlusion provocations at **II, III, IV**. The amount of hemoglobin changes during these occlusions and for hemoglobin optical absorption dominates over scattering [2]. Again, we are considering the elastic scattering in this context and it agrees with the fact that at 730nm the scattering was higher than that at 810nm.

Molar Concentration

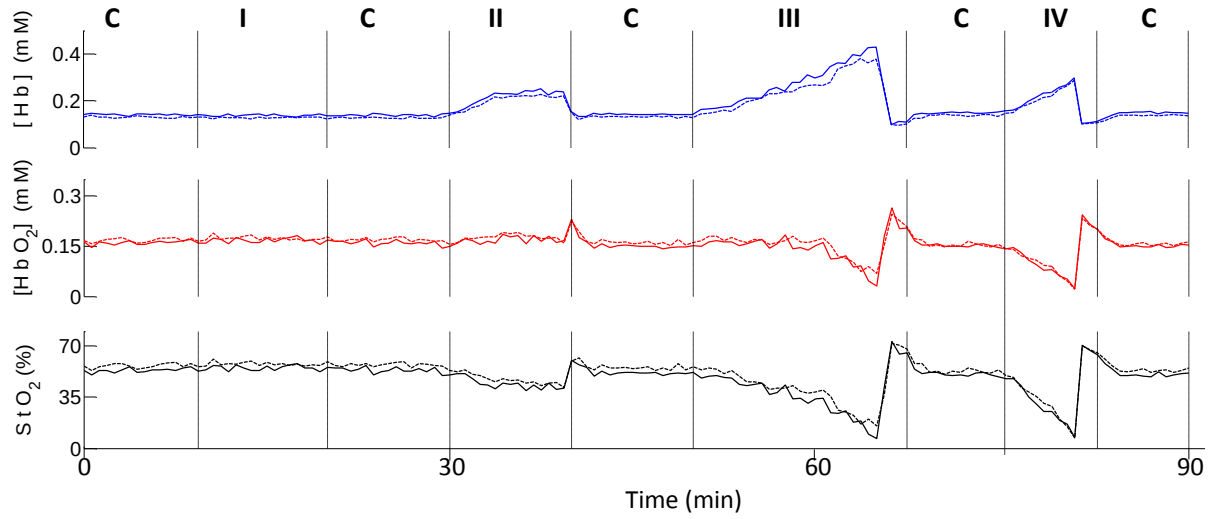

Figure 7.3: Molar concentration of de-oxygenated ([Hb]) and oxygenated ([HbO_2]) and the corresponding tissue saturation (StO_2) for 30 mm (solid lines) and 40 mm (dashed lines) for one volunteer using pTOFS [30]

The Figure 7.3 shows that the molar concentration of Hb increases in situation **II, III,** and **IV** at both distances. This is because the amount of Hb is increased for **II** where the venous blood is occluded at 60mmHg. At **III** the molar concentration increases gradually as the amount of Hb increases gradually. Molar concentration is related to the absorption coefficient and it is shown in Figure 7.3 that absorption coefficient is higher at 730nm for Hb. Thus all three situation shows rise in concentration.

It is noticeable that the tissue saturation is increased when the molar concentration of HbO_2 is increased. This is very much obvious as the tissue saturation StO_2 (%) reveals the oxygen binding to the Hemoglobin.

Tissue Saturation (StO_2) from pTOFS

The StO_2 values can be plotted as bellows:

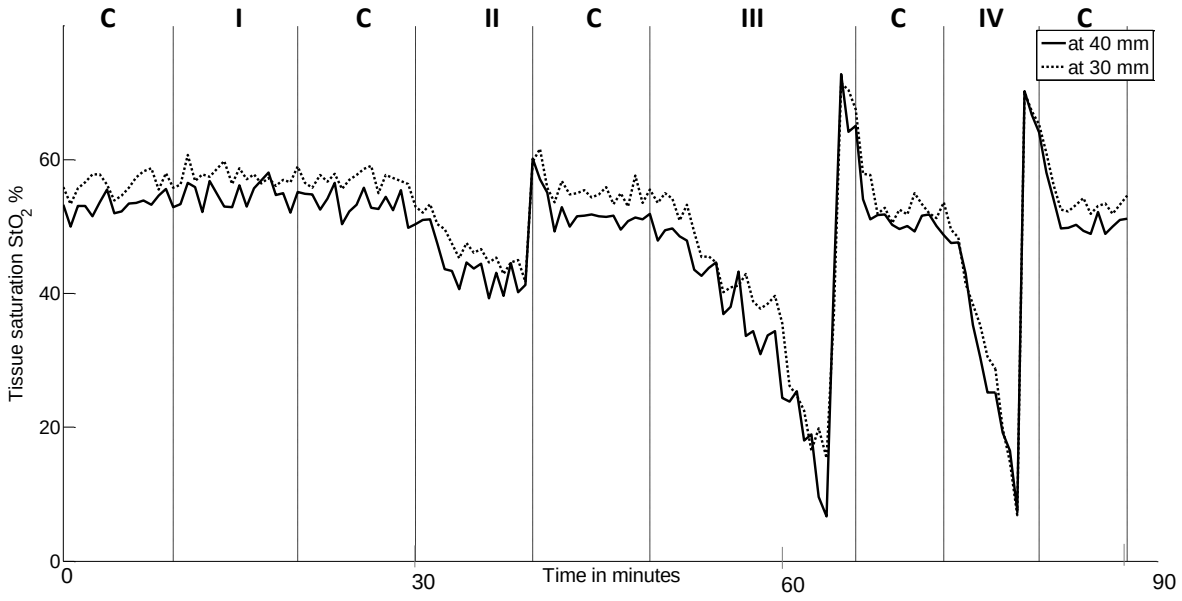

Figure 7.4: Tissue saturation measured from pTOFS (For one volunteer) measured at 40mm (solid line) and 30mm (dashed line)

It is clear from the Figure 7.4 that the pTOFS shows almost the same result at two distances, whereas the StO_2 values from the two CW-NIRS sensors differs in a wide range (See Figure 7.1). Another important aspect of pTOFS is that it can measure very low saturation at a pressure of 150mmHg (See **IV** and the last step of **III**).

The three minutes (approximately) just after releasing the cuff shows reactive hyperemia (A transient effect in the increment of tissue saturation just after the release of an arterial occlusion).In both the cases of **III** and **IV,** the sharp peak after the lowest point (last point of 150 mmHg) in the StO_2 (%) curve shows how quick the response is. When the cuff is released there is excess amount of oxygenated blood flow and thus the concentration of oxygenated blood (HbO_2) increases, while the concentration of de-oxygenated blood decreases.

7.3 Comparative Statistical analysis between pTOFS and CW-NIRS:

Standard Deviation:

The spreading from average data points for the two different techniques is shown. Figure 7.5 shows such dispersion (Shaded area) from the average for pTOFS (pTOFS 30 mm and pTOFS 40mm) and for CW-NIRS.

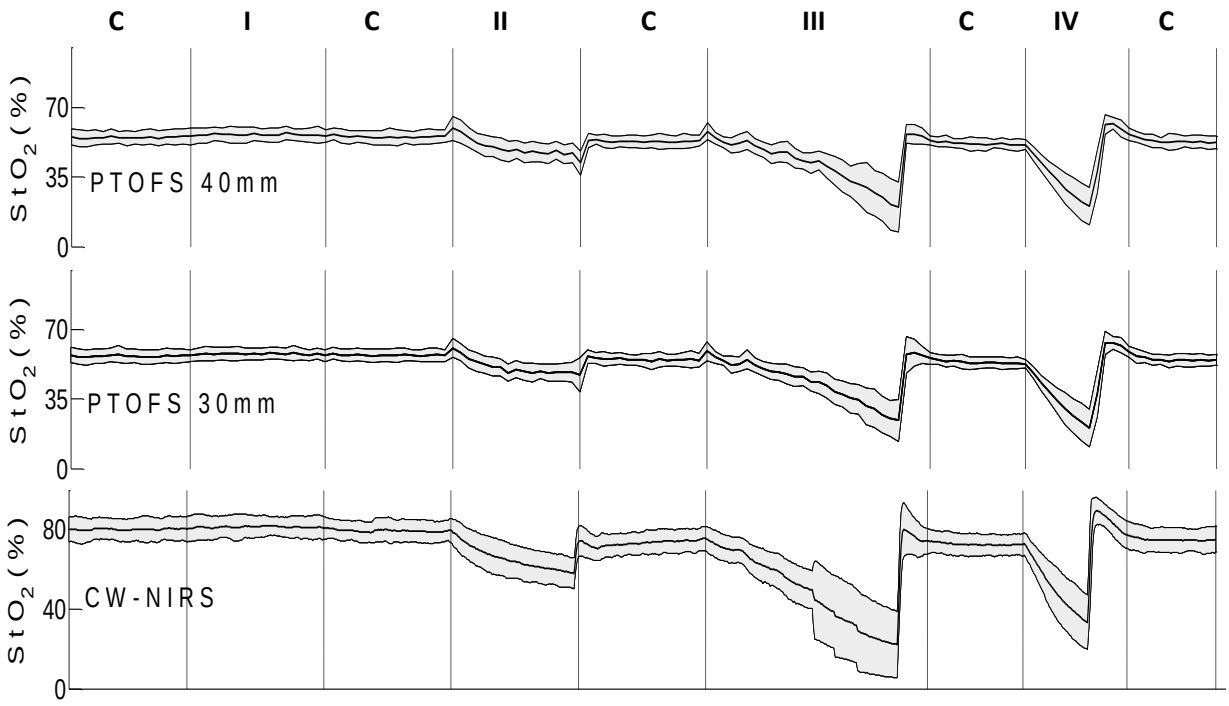

Figure 7.5: Average Tissue saturation StO_2 in % (Solid line) and Standard Deviation (Shaded area) for pTOFS and CW-NIRS [26]

It is quite clear from Figure 7.5 that the dispersion or spreading from the average value is much higher in CW-NIRS in comparison to pTOFS. It means the data points are very close to the mean value in case of pTOFS. So, it can be concluded that despite of different skin colors pTOFS shows StO_2 values which are more clustered around the average value.

Student ttest:

From Figure 7.6 it is clear that every provocation is followed by a resting position or baseline. A **ttest** was performed between an occlusion and the baseline prior to it. It is very interesting to show how significantly different the baselines are from different provocations for the two techniques. The results of such test are shown below in bars where the numbers on top of each bars shows the number of volunteers who showed significantly different values.

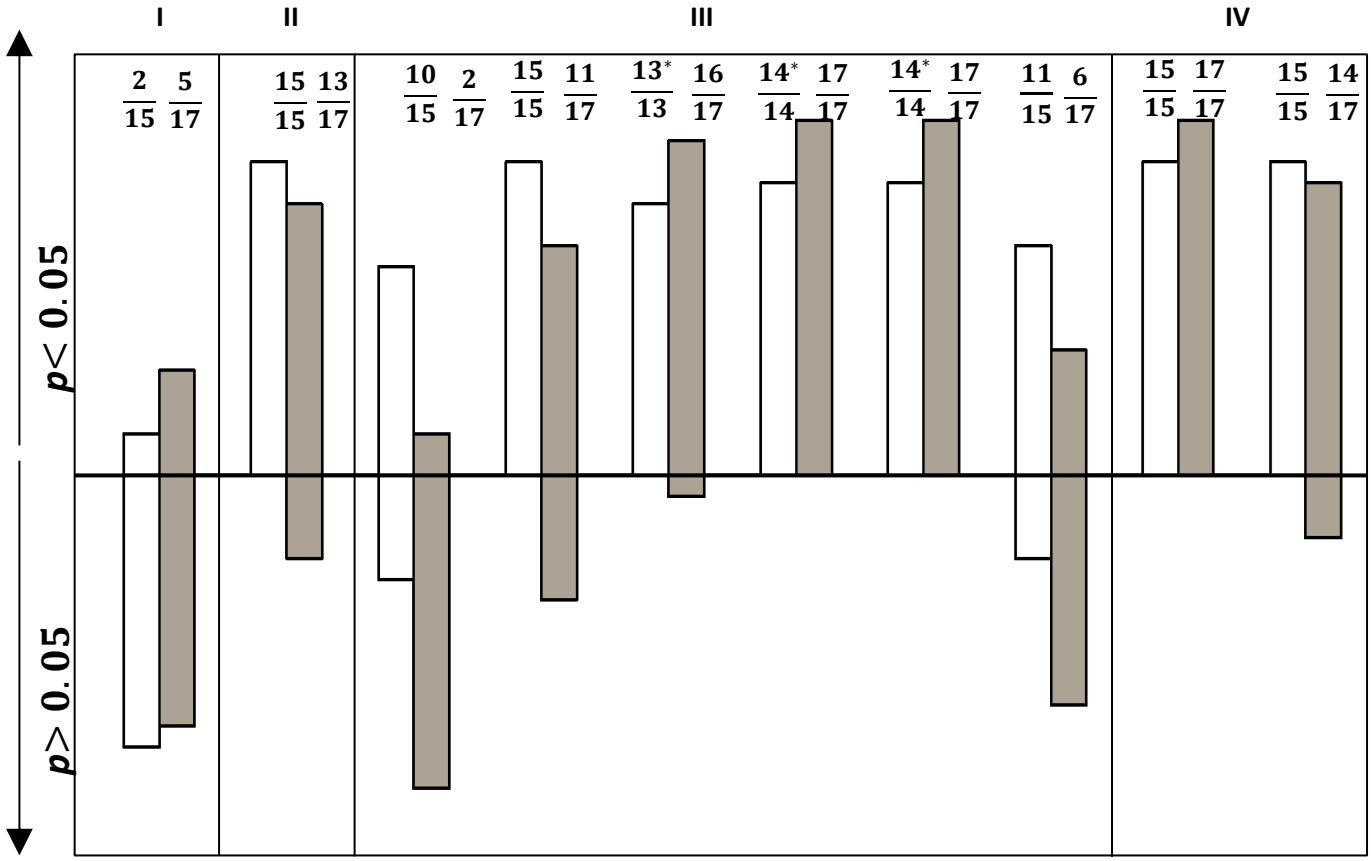

* Some of the StO_2 values for CW-NIRS system were not possible to analyze statistically as they had zero values

Figure 7.6: A histogram illustrating the results for the two techniques, CW-NIRS (White bars) and pTOFS (Grey bars) is shown. This presents how many volunteers (total 15 for CW-NIRS and 17 for pTOFS) showed significantly different values of tissue saturation during the provocations as compared to the corresponding values of the baseline prior to them; $p< 0.05$ corresponds to significantly different values and the opposite when $p> 0.05$ [26]

The white bars correspond to CW-NIRS system and the grey bars show the combined result from both the pTOFS results (pTOFS 30 and pTOFS 40). The combination is done in such a way that the volunteer showing p value<0.05 (significantly different) at one distance is considered to be different at both the distances.

It is quite evident from Figure 7.6 that StO_2 values change significantly for the highest occlusion for both cases and these corresponds to the second to last bars in **III** and **IV** .However it shows less difference in the first provocation which corresponds to the bars in **I.** The same for the first step of gradual occlusion of 30 mmHg i.e. the first bars of **III.** Generally an occlusion of 60mmHg should show significantly different values from its prior baseline, but for pTOFS 13/17 and 11/17 show different values for immediate and gradual occlusion (**II** and second step of **III**) respectively. Also for 90mmHg one would expect show different values for StO_2, which is true for 16/17. For the few exceptional cases we could conclude that the provocations were not applied properly during the measurement. The last steps of **III** and **IV** reflects difference of the reactive hyperemia from the baseline. It clearly shows significantly different values when the occlusion was immediate i.e. for **IV.**

Chapter 8

Conclusion

Tissue hypoperfusion i.e. reduction in blood flow through various important organs can lead to organ dysfunction and consequently death. An important goal of tissue saturation monitoring is the early detection of inadequate supply of oxygen. The thesis study was aimed to do a comparative study of the tissue saturation measurement (StO_2) between a newer and advanced system of pTOFS with a widely used CW-NIRS technique. In both techniques the ability to detect physiological changes with respects to StO_2 in human muscle tissue was achieved. Values of StO_2 based on both absorption and scattering effect can be achieved using the CW-NIRS system while pTOFS provides absolute values of StO_2 based on only absorption effect. The unique ability of pTOFS to separate these two effects provides smaller standard deviation (Figure 7.6) and the StO_2 values differ in a smaller range for the two distances of measurement. The values of StO_2 from pTOFS for resting position are in the range 55-60 %, whereas CW-NIRS gives values around 70-90 %. The StO_2 values from CW-NIRS thus much higher, nearly matching the arterial oxygen saturation [28]. The values achieved from both the systems are expected to mostly reflect the venous saturation, as over 70% of the total blood volume is found in the venous part of the tissue [29].

Despite only providing relative values, CW-NIRS is a very handy to use and is available on the market, though the values can vary from instruments to instruments [30]. On the other hand pTOFS instrumentation still requires more research to be used for clinical measurement.

Appendices

Table1: StO_2 (%) values from one sensor for CW-NIRS (one volunteer)

C	I	C	II	C			III			C	IV	C
88	92	87	84	79	82	69	53	0	0	74	70	62
88	92	87	83	83	82	68	53	0	0	80	69	91
88	92	87	82	83	81	66	53	0	0	80	68	95
88	93	87	81	82	81	66	51	0	0	78	66	95
89	93	87	80	82	80	64	50	0	0	75	65	95
90	93	87	79	81	79	63	50	0	0	73	63	95
90	93	87	78	80	79	62	48	0	0	72	61	95
90	93	87	77	79	78	61	48	0	0	70	60	95
90	92	87	75	78	77	60	48	0	0	68	58	95
89	92	87	74	77	77	59	47	0	0	68	56	95
89	91	87	73	76	76	58	46	0	0	67	55	95
89	91	87	72	75	76	58	46	0	0	68	53	95
88	91	87	70	74	75	58	46	0	0	68	52	95
88	91	86	69	74	74	56	45	0	0	68	50	95
88	90	85	68	75	73	55	46	0	0	68	49	95
87	90	84	67	75	72	56	45	0	0	67	47	95
87	90	84	66	76	72	57	47	0	0	67	46	95
86	89	83	65	75	71	57	46	0	0	68	44	95
86	89	82	64	75	71	57	46	0	0	68	43	95
86	89	82	63	75	70	56	46	0	0	69	41	95
86	89	82	63	75	69	57	46	0	0	70	40	95
86	89	82	63	76	69	55	45	0	0	71	38	95
87	88	81	62	75	69	56	45	0	0	72	37	94
88	88	81	62	75	69	56	45	0	0	73	35	94
88	88	81	62	75	70	56	0	0	0	73	34	93
89	88	80	62	75	70	55	0	0	0	74	32	93
89	88	80	61	75	71	55	0	0	0	74	31	92
89	88	80	61	75	71	55	0	0	0	75	30	91
89	88	80	60	75	71	56	0	0	0	75	29	90
90	88	79	60	75	69	55	0	0	44	75	27	89
89	89	79	60	75						75	26	89
89	90	79	60	75						75	24	88
89	91	78	59	75						75	23	88
89	91	78	59	76						74	22	87
88	92	77	59	76						75	20	86
88	92	78	58	77						76	20	86
88	92	78	58	77						76	18	85
88	92	78	58	76						77	15	85
88	93	77	58	76						77	15	85
88	92	79	58	76						77	15	85

88	92	83	58	76		77	15	85
88	92	88	58	76		76	15	85
88	91	90	57	76		76	15	84
88	91	91	57	76		76	15	83
87	91	92	57	76		75	15	83
87	90	91	56	76		75	15	83
87	90	91	56	77		75	15	83
88	89	91	56	77		76	15	82
88	89	91	56	76		75	15	83
88	88	90	55	76		75	15	83
88	88	89	56	76		75	62	84
88	88	88	55	77		75		84
89	87	87	56	77		75		85
88	87	86	55	77		75		85
89	87	85	55	78		74		85
89	88	84	54	79		74		85
90	88	83	54	80		74		85
90	88	82	54	80		74		84
90	88	81	54	79		74		84
91	87	80	54	79		75		83
91	87	80	56	80		75		83
91	87	80	56	80		75		83
91	86	79	55	80		74		83
91	86	79	54	81		74		82
91	85	79	54	81		74		81
91	85	80	53	82		75		81
91	85	79	52	82		75		81
90	85	79	52	82		75		81
90	85	79	53	81		76		80
89	85	79	53	81		76		80
89	86	79	51	80		76		80
89	86	80	52	80		76		80
88	86	80	52	79		76		80
88	86	81	51	78		75		80
88	86	82	52	77		75		80
88	86	82	52	77		75		80
88	87	82	52	76		75		79
87	87	81	52	75		75		79
87	87	81	52	75		74		79
87	87	81	54	76		74		80
87	88	80	53	78		74		80
86	88	81	54	78		74		81
86	88	81	54	78		74		82
86	88	81	53	78		74		82
86	87	81	53	79		74		83
86	87	82	52	79		75		83
86	87	81	51	79		75		83

86	86	81	50	79		77		83
86	85	82	51	79		77		83
85	85	83	49	78		77		83
85	85	85	50	78		76		82
85	85	86	50	77		76		82
85	86	87	49	76		76		82
86	87	87	50	76		76		82
88	87	86	49	76		75		82
89	88	86	51	78		75		82
90	88	86	51	80		74		82
91	88	85	51	81		73		81
91	88	84	52	83		72		81
92	88	84	62	83		70		81

Table2: StO_2 (%) values from one volunteer for pTOFS at 30 mm

C	I	C	II	C			III			C	IV	C
53.00	56.00	54.00	55.00	40.00	57.00	50.00	42.00	31.00	25.00	31.00	49.00	29.00
49.00	56.00	55.00	58.00	53.00	53.00	48.00	41.00	38.00	18.00	60.00	47.00	64.00
54.00	55.00	54.00	54.00	53.00	51.00	46.00	41.00	30.00	15.00	64.00	41.00	64.00
51.00	55.00	53.00	48.00	52.00	50.00	45.00	35.00	28.00	6.00	62.00	36.00	59.00
53.00	56.00	55.00	49.00	50.00	49.00	45.00	39.00	25.00	7.00	51.00	30.00	59.00
53.00	54.00	53.00	46.00	51.00						51.00	26.00	52.00
54.00	54.00	52.00	46.00	53.00						54.00	25.00	50.00
55.00	55.00	52.00	43.00	50.00						50.00	19.00	51.00
52.00	55.00	56.00	45.00	52.00						51.00	16.00	49.00
53.00	54.00	54.00	41.00	51.00						49.00		49.00
55.00	57.00	52.00	45.00	52.00						50.00		49.00
51.00	57.00	52.00	41.00	50.00						50.00		51.00
56.00	55.00	55.00	37.00	51.00						52.00		49.00
53.00	55.00	52.00	43.00	51.00						51.00		52.00
55.00	53.00	52.00	42.00	51.00						49.00		50.00
54.00	54.00	53.00	41.00	52.00						49.00		50.00

Student t test :

A ***t*-test** is a test that performs some hypothesis test on samples where the statistic follows a ***t*** distribution if the null hypothesis is supported. Paired ***t*-test** is done when the two samples to be compared are not arbitrarily chosen rather the second sample is the same as the first after some action has been applied on it. Give two these types of samples, the situation can basically reduce to whether the mean of each samples overlap or if they do not overlap. In which case the

means could be the same we *may not* reject the null hypothesis that the difference in mean values for the paired observations is zero while we must reject the null hypothesis for the case where the difference is not zero. The results are either the means are not "significantly" different or means are "significantly" different. The probability of the outcome under the hypothesis that the means are the same is equal to *p*-value. When the *p*-value is less than a predetermined significance level, which is often 0.05 or 0.01, the null hypothesis is rejected.

References

1. Svanberg, S., [*Atomic and Molecular Spectroscopy*], Springer (2001).
2. Wang, Lihong V., Wu , Hsin-I, [*Biomedical Optics, Principles and Imaging*], Wiley –Interscience , Chapter 1 (2007).
3. Svensson , T., [Pharmaceutical and Biomedical Applications of Spectroscopy in the Photon Migration Regime], PhD thesis, Division of Atomic Physics Department of Physics, Faculty of Engineering, LTH, Lund University, P.19-22(2008).
4. Alerstam, E. ,[*Optical Spectroscopy of Turbid Media: Time Domain Measurements and Accelerated Monte Carlo Modeling*]. PhD thesis, Lund University (2011).
5. Saxena[1], V., Marcu[2], L., Karunasiri[3], G., "*A novel noninvasive all optical technique to monitor physiology of an exercising muscle"*, Phys Med Bio, 53(21):6211-25(2008 Nov 7).
6. <http://omlc.ogi.edu/spectra/hemoglobin>
7. Svanberg, E., K. , Wollmer, P., Andersson-Engels, S., Åkesson, J., "*Physiological influence of basic perturbations assessed by non-invasive optical techniques in humans",* Can. J. Appl. Physiol., 36(6), 946-957 (2011).
8. *<http://www.somanetics.com/invos-system>*
9. *<http://www.arpansa.gov.au/pubs/RadiationProtection/FitzpatrickSkinType.pdf\>*
10. *<http://www.rp-photonics.com/photonic_crystal_fibers.html>*
11. Anderberg,V., [*Near Infrared Spectroscopy for measuring Optical Parameters in Flour and Grain*], Master's thesis Lund University Faculty of Engineering, LTH June 2009.
12. Saleh ,B.E.A. , Teich ,M.C.,[*Fundamental of Photonics*], Wiley series in Pure and Applied Optics (2007).
13. Fianium Ltd. ,[Manual for femto power 1060, tunable super continuum source, sc450-AOTF].
14. *<http://www.micro-photon-devices.com/media/pdf/PDM.pdf>*
15. [SPC-handbook, 5th Edition]
16. Subash,A.A.,[*WIDE-BANDWIDTH TIME OF FLIGHT SPECTROSCOPY OF TURBID* MEDIA], Master's *Thesis,* Lund University Faculty of Engineering, LTH January 2012.
17. Ishimaru ,A., [*Wave Propagation and Scattering in Random Media*], ACADEMIC PRESS,INC, New York, Chap. 7, p. 157; Chap. 9, p. 17(1978).
18. Khoptyar, D. , Saleem, M. , Subash, A.A. , Andersson-Engels, S. ," *Wide Bandwidth Time of Flight Spectroscopy of Turbid Media*," III International Symposium on TOPICAL PROBLEMS OF BIOPHOTONICS – 2011, St.-Petersburg- Nizhny Novgorod, Russia, Page 57-58(2011).
19. Contini, D., Martelli,F., and Zaccanti,G.," *Photon migration through a turbid slab described by a model based on diffusion approximation. I. Theory*," Appl. Optics, 36(19), 4587-4599 (1997) .

20. Marqardt ,D.W.,"*An algorithm for least squares estimation of nonlinear parameters"* J.Soc.Indust. Appl.Math., 11(2),431-441(1963)

21. Alerstam,E., Andersson-Engels, S., Svensson, T.," *White Monte Carlo for time-resolved photon migration."* JBiomedOpt.,13(4),(2008) .

22. <http://www.atomic.physics.lu.se/fileadmin/atomfysik/Education/Elective_courses/Medical_optics/Tissue_Optics_2011_-_Lab_-_Time_Resolved_Spectroscopy_.pdf>

23. Germon, T., J., Evans, P., E., Barnett, N., J., Lewis, T., T., Wall,V., Nelson, R., J.,"*Changes in tissue oxyhaemoglobin concentration measured using multichannel near infrared spectroscopy during internal carotid angiography*," J Neurol Neurosurg Psychiatry, 63(5),660-4(1997).

24. <http://www.atomic.physics.lu.se/education/elective_courses/faf150_medical_optics/>

25. <http://www.somanetics.com/our-technology/product-and-accessories>

26. Svanberg,E.,K., Shaharin, A., Ellerström,I., Subash,A.,A., Khoptyar,D., Andersson-Engels,S., and Åkeson,J.," *Time-resolved versus continuous wave near-infrared spectroscopy for determination of oxygen saturation in human skeletal muscle tissue,"* Manuscript is in progress.

27. Groothuis JT, van Vliet L, Kooijman M, Hopman MT. ,"Venous cuff pressures from 30 mmHg to diastolic pressure are recommended to measure arterial inflow by plethysmography, " J Appl Physiol ,95(1):342-7(2003).

28. Franceschini MA, Gratton E, Fantini S."*Noninvasive optical method of measuring tissue and arterial saturation: an application to absolute pulse oximetry of the brain,"* Opt Lett.,24(12),829-31(1999).

29. Paradis, N., A., Halperin, H., R., Kern, K., B.,[*Cardiac Arrest: The Science and Practice of Resuscitation Medicine*] , Cambridge University Press, Chapter 17 , Page 348(2007).

30. Hyttel-Sorensen S, Sorensen LC, Riera J, Greisen G." *Tissue oximetry: a comparison of mean values of regional tissue saturation, reproducibility and dynamic range of four NIRS-instruments on the human forearm,"* Biomed Opt Express. , 2(11), 3047–3057(2011).

31. Cui, W.J., Kumar, C. ,and Chance, B. ,"Experimental-Study of Migration Depth for the Photons Measured at Sample Surface, " Proc. SPIE Vol. 1431, p. 180-191(1991).

32. Edwards Life Sciences, [*Understanding continuous mixed venous oxygen saturation, Monitoring with Swan-Ganz oximetry TD system.]* 2nd Edition .

33. Hölzle F, Loeffelbein DJ, Nolte D, Wolff KD. ,"*Free flap monitoring using simultaneous non-invasive laser Doppler flowmetry and tissue spectrophotometry,"* J Craniomaxillofac Surg. ,34(1):25-33(2006).